Petrology of Komatiites from the Baltic Shield and Isotope Geochemical Evolution of Their Mantle Sources

A. B. Vrevsky, V. A. Matrenichev, and M. S. Ruzh'eva

Institute of Precambrian Geology and Geochronology, Russian Academy of Sciences, nab. Makarova 2,
St. Petersburg, 199034 Russia; e-mail: vrev@AV3213.spb.edu
Received March 8, 2003

Abstract—This paper presents the results of investigations of the geochemical and isotopic compositions of komatiites from various Late Archean greenstone belts and structures of the Baltic shield. The analysis of major, trace, and rare earth elements demonstrated a considerable heterogeneity of their composition and lateral zoning in the distribution of their characteristics. It was found that variations in the contents of FeO, Al_2O_3, MgO, and REE and Al_2O_3/TiO_2, Ti/Zr, Y/Zr, $(Ce/Sm)_N$, and $(Gd/Yb)_N$ ratios in the complexes studied are related to various factors and have diverse origins. In order to decipher the latter, isotope geochemical data and methods of petrological and geochemical modeling of rock-forming processes were applied. The analysis of regularities in the spatial and temporal distribution of greenstone belts, the lithological characteristics of volcanosedimentary complexes, and the geochemical and isotopic heterogeneities of komatiites and their mantle sources demonstrated that they can be most adequately interpreted by the model of development of two mantle plumes of different ages.

INTRODUCTION

The postaccretion geologic history of the Earth is represented by Archean (>2.5 Ga) rock complexes, which occur in the epi-Archean cratons of ancient continents, whose lithosphere was formed mainly in tectonic terranes of two main types, granite–greenstone and granulite–gneiss. The most comprehensive data for the first billion years of the existence of the continental crust can be gained from the investigation of the tectonic settings of formation and development of Archean greenstone belts, because they are characterized by relatively low degrees of secondary alteration and spatial and temporal juxtaposition of large volumes of derivatives of mantle and crustal magmatism, the oldest stromatolites, iron formation, and manganese ore complexes. Komatiites play a key role in the reconstruction of the structure and composition of the upper mantle and the estimation of thermodynamic conditions in the Early Precambrian lithosphere. Because of the occurrence of these rocks mainly in Archean greenstone belts and their ultrabasic (MgO > 24 wt %) varieties only in them, the investigation of komatiites is of paramount importance for the understanding of isotopic geochemical and thermal evolution of the mantle at early stages of Earth evolution.

The goal of our study was to explore the geochemical and isotopic compositions of komatiites from the Archean greenstone belts of different ages of the Baltic shield and their mantle sources and to determine quantitative petrological and geochemical model constraints on the conditions of primary komatiitic melt segregation from mantle sources.

GEOLOGY OF THE ARCHEAN GRANITE–GREENSTONE TERRANES OF THE BALTIC SHIELD

The Archean granite–greenstone terranes of the Baltic shield (Karelian and Kola) are composed of a number of greenstone (volcanosedimentary) structures and belts (Fig. 1a) surrounded by fields of tonalite-trondhjemite gneisses, granites, and granulite gneisses.

The volcanosedimentary structures of greenstone belts are combined into the Lopian complex in the regional stratigraphic scale of the Baltic shield. The sections of Lopian greenstone belts are in general characterized by variability in the facies, proportions, and thicknesses of sedimentary and volcanic complexes (Fig. 1c). Since the rocks of greenstone belts experienced at least two stages of structural and metamorphic transformations, the sections presented show only the principal structure, sequence of lithologic units, and compositions of Lopian supracrustal complexes.

All the major lithologic types of sections of Early Precambrian greenstone belts have been distinguished in the respective structures of the Baltic shield. Three types of the lower parts of Lopian sections corresponding to the initial stages of greenstone belt development were detected: (a) terrigenous, (b) calk-alkaline, and (c) komatiite–tholeiite. Bimodal and polymodal types of endogenous evolution were also documented in these structures (Vrevsky *et al.*, 1996).

In the modern erosion level, the greenstone belts of the Karelian and Kola geoblocks of the Baltic shield show in general different orientations (trending approximately N–S and NW, respectively), but the paleotec-
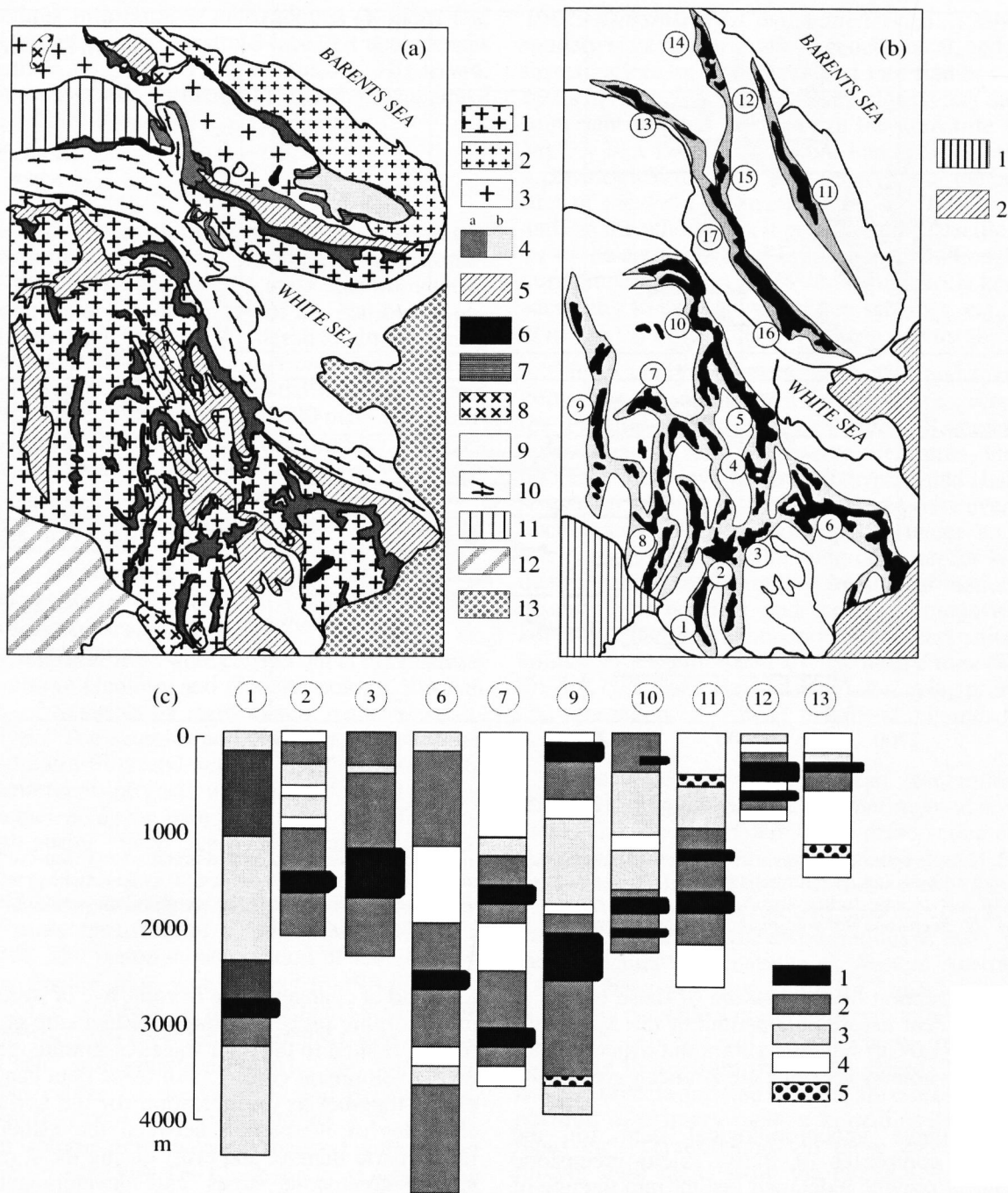
Fig. 1. (a) Schematic geologic structure of the eastern Baltic shield, (b) paleotectonic reconstruction of Archean greenstone belts, and (c) their generalized stratigraphic sections (Vrevsky *et al.*, 1996).

(a) (1)–(3) Undifferentiated Archean ($AR_1 + AR_2$) complex of tonalite–trondhjemite gneiss, granite, migmatite, and granulite in (1) Fenno–Karelian and (2), (3) Kola–Norwegian provinces; (4) Lopian (AR_2) complex (a, greenstone belts and b, Keivy paragneiss structure); (5) Sumian–Sariolian and Jatulian (PR_1) complexes; (6) basic–ultrabasic layered intrusions (PR_1); (7) peralkaline granite (AR_2); (8) rapakivi granite (PR_2); (9) nepheline syenite (PZ); (10)–(13) tectonic complexes: (10) Belomorian belt (2.4–1.8 Ga), (11) Lapland–Kolvitsa granulite belt, (12) Svecofennides, and (13) Phanerozoic platform cover.

(b) (1) Svecofennides; (2) Phanerozoic platform cover. Numerals in circles are Archean greenstone belts and structures: 1–4, Vedlozero–Segozero belt (1—Hautavaara, 2—Koikari, 3—Palaya Lamba, and 4—Sovdozero structure); 5, Parandovo; 6, Kamennoozero; 7, Kostamuksha; 8, Yalonvaara; 9, Kuhmo–Suomussalmi; and 10, Hizovaara structures; 11, 12, Kolmozero–Ura Guba belt (11—Polmos-Porosozero and 12—Ura Guba structure); 13, Korva Tundra structure; 14–17, Tersk-Allarechka belt (14—Kaskama, 15—Olenegorsk, 16—Tersk, and 17—Ingozero structures).

(c) (1) Komatiite; (2) basalt; (3) andesite and dacite; (4) sediment; (5) conglomerate. Numerals in circles are Archean greenstone belts and structures (Fig. 1b).
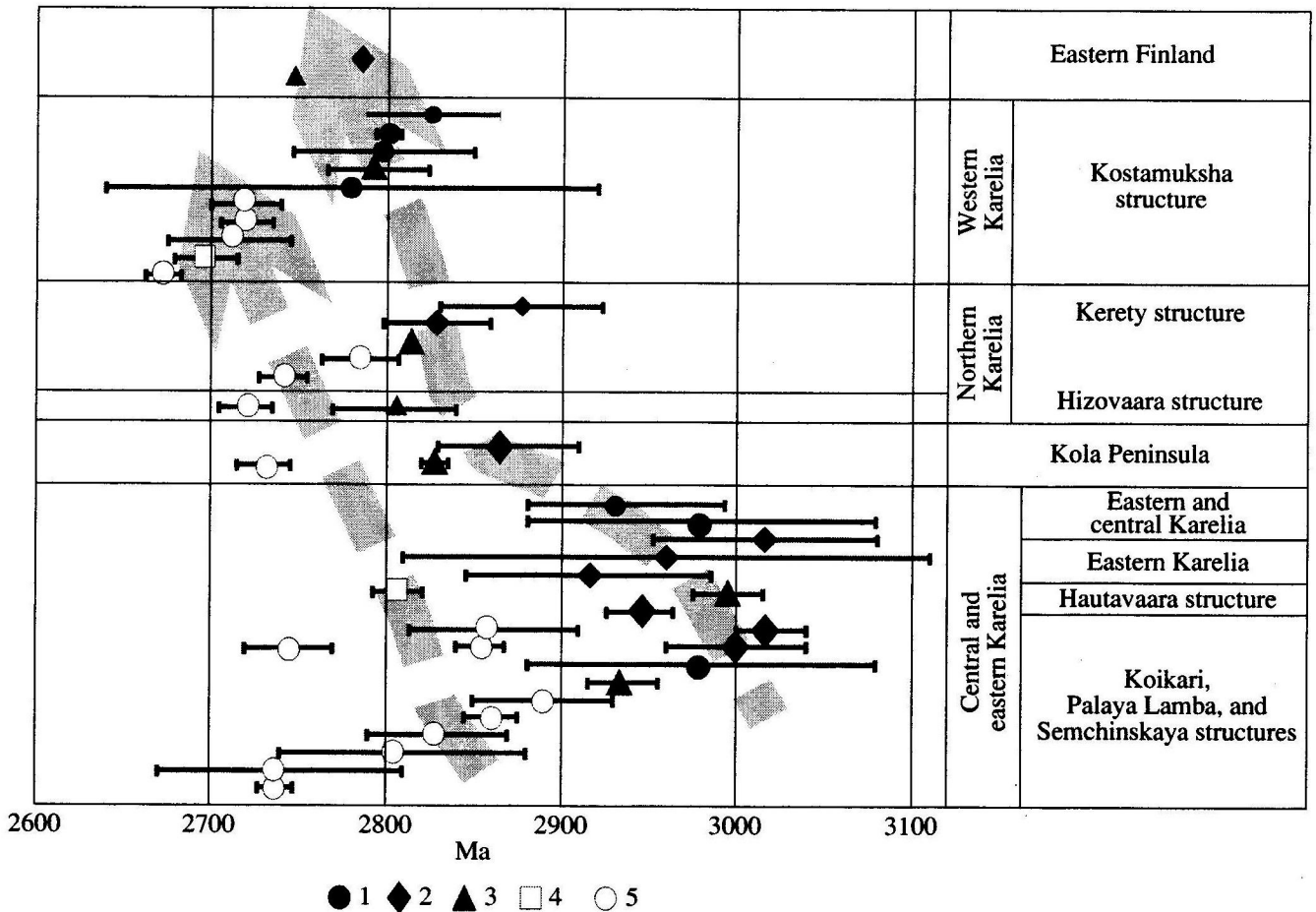
Fig. 2. Isotopic ages of volcanism in the Archean greenstone belts of the Baltic shield and related granitoids. (1) Sm–Nd age for bulk rocks (komatiites and basalts); (2)–(5) U–Pb isotopic ages for zircons: (2) andesites, (3) dacites, (4) synkinematic granites and dikes of postvolcanic dacites, and (5) postkinematic granites and age of metamorphism. The dashed arrows show trends of "rejuvenation" of greenstone belt volcanism and related granitoids.

tonic reconstruction of the position of these blocks at the time moment before the opening of the Kandalaksha graben (~1.0 Ga) suggests a common structural pattern for the whole system of Late Archean greenstone belts (Fig. 1c).

The available geochronological data for the supracrustal complexes of Baltic shield greenstone belts (Fig. 2) provide a detailed insight into the age of volcanism and the time of the last structural and metamorphic transformations and allow us to estimate the duration of formation of some belts and structures. Three age groups of greenstone belts volcanism were distinguished on the basis of these data in the age interval ~3.1–2.65 Ga (Fig. 2):

—2.9–3.05 Ga, central and eastern Karelia;

—2.8–2.9 Ga, Kola Peninsula and northern Karelia; and

—2.75–2.8 Ga, eastern Finland and western Karelia.

The age trend of volcanic processes at the initial stages of greenstone belt formation is in general regularly paralleled, with a displacement by ~100 m.y., by

the trend of changes in the isotopic age of structural and metamorphic processes and postkinematic granite formation related to the final stages of granite–greenstone belt development (Fig. 2). All these data can be interpreted together as an indication for the asynchronous character of interaction between the asthenosphere, lithospheric mantle, and crust during the formation of granite–greenstone areas and development of the Archean lithosphere of the Baltic shield as a whole (Vrevsky *et al.*, 1996; Vrevsky and Krymsky, 1997).

Komatiitic magmatism is rather widespread in a number of greenstone belts and structures and may account for up to 10–15 vol % of the volcanogenic part of their sections (Fig. 1c). These volcanic objects are characteristic of the Early Precambrian and are usually confined to the lower, predominantly volcanogenic, parts of sections of Lopian volcanosedimentary complexes, except for the Hautavaara structure, where they were preceded by an andesite–dacite volcanic cycle. The investigations of many years of greenstone belt volcanism allowed us to reconstruct relict paleovolca-

nic structures in a number of structures (Koikari and Palaya Lamba) and demonstrate repeated occurrences of komatiitic magmatism (Kostamuksha, Hizovaara, and Suomussalmi structures) (*Zelenokamennye poyasa...*, 1988; *Komatiity i...*, 1988; etc.).

ANALYTICAL METHODS

Trace and rare earth elements (REE) were determined by inductively coupled plasma mass spectrometry (ICP-MS) on an MSGV-354 mass spectrometer at the Laboratory of Geochemistry of the National Geophysical Research Institute (Hyderabad, India) using the procedure described by Jahn *et al.* (1980) with an analytical error of 5% for HREE and 3% for LREE, and on a Perkin Elmer SCIEX ELAN 5000 mass spectrometer at Granada University (Granada, Spain). Charges of 0.1 g were treated for 150 min with $HNO_3 + HF$ mixtures in Teflon-lined vessels at high temperature and pressure, dried, and then dissolved in 4% HNO_3. Mass spectrometric measurements were carried out three times using Rb, Re, and In as internal standards. The analytical uncertainties were 2 and 5 rel. % for concentrations of 50 and 5 ppm, respectively.

Some measurements were carried out at the Institute of Precambrian Geology and Geochronology, Russian Academy of Sciences by instrumental neutron activation analysis. The samples and standards were loaded into a cadmium filter and neutron-irradiated for 50 h. The measurements of γ activity were performed using a 4095-channel analyzer with a detector manufactured from high-purity "ideal" germanium and a Ge-(Li) detector.

Sm–Nd isotopic analysis was carried out on an 8-collector mass spectrometer Finnigan MAT-261 in a static mode. The isotopic composition of Nd was corrected for fractionation with respect to $^{148}Nd/^{144}Nd = 0.241570$. The accuracy of measurements was ±0.5% for $^{147}Nd/^{144}Nd$, ±0.005% for $^{143}Nd/^{144}Nd$, and 1% for Sm and Nd concentrations (2σ). The measured $^{143}Nd/^{144}Nd$ values for the La Jolla and BCR-1 standards were 0.511864 ± 14 and 0.512668 ± 15, respectively. Nd isotopic ratios were normalized with respect to $^{146}Nd/^{144}Nd = 0.7219$. The blank run level was 0.3 ng for Sm and 0.5 ng for Nd. Some measurements were obtained at the National Geophysical Research Institute (Hyderabad, India) on a VG-262 mass spectrometer with higher analytical parameters using the same procedures of sample preparation and processing of measurements.

CHEMICAL CHARACTERISTICS OF KOMATIITES

This paper is concerned mainly with the most magnesian varieties of the komatiite series (MgO > 18 wt %), which, according to the currently accepted classification, are classed as komatiites proper (*Komatiites,*

1982; *Klassifikatsiya magmaticheskikh...*, 1997). The modern state of petrological, geochemical, and isotopic investigations of komatiites and rare findings of these rocks in Phanerozoic complexes suggest that there is an important internal boundary in the komatiite series at MgO = 24 ± 1 wt %. On the one hand, this boundary has a petrological meaning as a reflection of the composition of the *Fo–Di* cotectic in the *Fo–Di–Qtz* system; and, on the other hand, it points out the specific character of the early stages of lithosphere evolution, because komatiites with MgO > 24 wt % (peridotitic komatiites according to early classification schemes, e.g., Nesbet *et al.*, 1977) occur only in Archean greenstone belts.

The primary magmatic structures and textures of komatiites are retained to a varying degree: very well in the Polmos–Porosozero, Ura Guba, Kamennoozero, Palaya Lamba, and Sovdozero structures and much poorer in the Korva Tundra, Hizovaara, and Hautavaara structures. However, spinifex textures were everywhere documented either in outcrops or under an optical microscope. This was the main criterion for komatiite distinguishing and sampling for the estimation of the primary geochemical and isotopic compositions of komatiitic melts. The mineralogical composition of the komatiites is dominated by secondary minerals (*Srp, Tr, Act, Chl, Cal ± Ilm* and *Mag*) in varying proportions and rare relics of primary magmatic minerals (*Ol, Px,* and *Spl*).

Since essentially all Archean komatiites were affected to a varying extent by superimposed processes, there is an urgent problem of the preservation of initial compositions in the petrogenetic and isotopic geochemical investigations of these rocks (this is also true for all other Precambrian igneous complexes). In the authors' opinion, the investigations of many years of the least altered komatiites of Western Australia and Canada have provided some fundamental inferences that made possible a correct interpretation of the isotopic and geochemical heterogeneity of komatiites including those from the Baltic shield. The zones of flowtop breccia and fine spinifex are closest to the composition of primary melt in komatiite flows, because rapid melt crystallization in these zones minimized mixing with melts from the cumulative and bottom parts of flows, which were often affected by assimilation and thermal erosion. The thinnest flows (up to 5 m) were usually least affected by assimilation processes.

Leaving aside the general problems of the isochemical nature of regional metamorphism, it can be stated that the most mobile in the processes of metamorphic transformations of komatiites are large ion lithophile elements, Cs, Rb, K, Na, Ba, Sr, and Eu^{2+}, and the least mobile are Mg, Cr, Fe, Mn, Ni, Co, Y, Zr, and Nb. In general, REE are low mobile elements during superimposed metamorphic alterations, and random variations in LREE contents and distribution patterns in komatiites due to carbonation and chloritization can be excluded by the petrographic control of sampling.
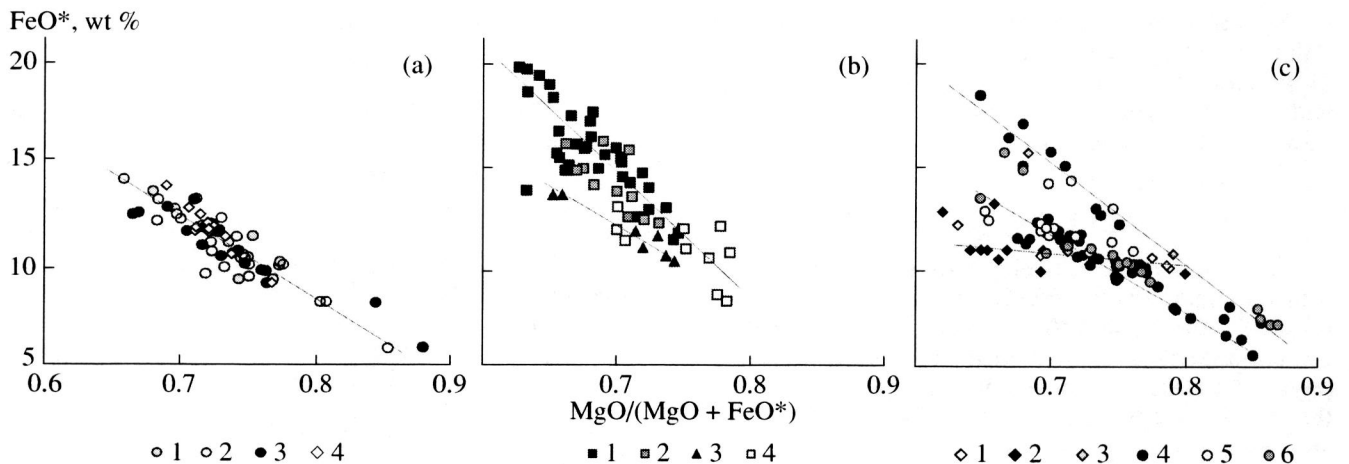
Fig. 3. Diagram FeO* versus MgO/(MgO + FeO*) for the komatiites of (a) central and eastern Karelia; (b) Kola Peninsula, northern Karelia, and western Karelia; and (c) other world regions.

(a) (1) Sovdozero; (2) Palaya Lamba and Koikari; (3) Kamennoozero; and (4) Hautavaara structures.

(b) (1) Polmos-Porosozero; (2) Ura Guba; (3) Kostamuksha; and (4) Hizovaara structures.

(c) (1) Suomussalmi structure; (2) Ilomantsi structure; (3) Kuhmo structure; (4) Canada; (5) South Africa; and (6) Western Australia.

These considerations limited the number of the major elements (SiO_2, Al_2O_3, MgO, and FeO) that were used for the determination of the most general regularities in the evolution of komatiite composition. In addition, variations in the contents of several incompatible elements (Ti, Zr, and Y) and REE distribution patterns correlated with Nd isotopic compositions were used for petrogenetic constructions and inferences.

Major and Trace Elements

The results of the investigation of petrochemical and geochemical characteristics of all known Archean komatiitic occurrences in the Baltic shield revealed a number of features and new regularities in the evolution of komatiite composition, which have a bearing on the lateral heterogeneity of komatiite magmas and their mantle sources and genetic features of primary komatiite magma generation.

A number of petrochemical diagrams presented in this paper show all published results on the compositions of Baltic shield komatiites together with our new analyses (~30% of the database) (Vrevsky *et al.*, 1996; Vrevsky and Krymsky, 1997). The most important supplement to the previous data is represented by new precise analyses of trace and rare earth elements in komatiites (Table 1), their isotopic geochemical systematics, and petrogenetic interpretation.

A comparison of the compositions of Baltic shield komatiites with representative analyses (>120) from similar complexes of the Archean greenstone belts of the Canadian, Zimbabwe, and Western Australian cratons revealed much more complicated regularities in the compositional evolution of the Baltic shield komatiites in comparison to two global types of komatiitic magmas, Al-depleted (Al_2O_3/TiO_2 ~ 10 and CaO/Al_2O_3 > 1.0)

and Al-undepleted (Al_2O_3/TiO_2 > 20 and CaO/Al_2O_3 < 1.0) (Arndt, 1994).

In general the Baltic shield komatiites show relatively widely varying major element contents with a number of significant regional and genetic differences.

The most significant variations were detected in the Mg# values of rocks; contents of SiO_2, Al_2O_3, and FeO* = FeO + 0.9Fe_2O_3; and Al_2O_3/TiO_2, Y/Zr, and Ti/Zr ratios.

The most iron-rich (FeO* = 12–19 wt %) are the komatiites of the Kola Peninsula (Polmos-Porosozero, Ura Guba, and Korva Tundra structures), which have only rare analogues among worldwide komatiites. The komatiites of the Kola Peninsula form an independent trend in the FeO*–MgO/(MgO + FeO*) coordinates. Most of the komatiites of the Hizovaara structure (northern Karelia) fall on the same trend at much lower iron content (Fig. 3b).

The komatiites of central Karelia (Vedlozero–Segozero greenstone belt) and eastern Karelia (Kamennoozero structure) usually show much lower iron contents and variations (FeO* = 7–13 wt %) accompanied by a relatively high Mg# (0.68–0.85) (Fig. 3a). In the FeO*–MgO/(MgO + FeO*) coordinates, they plot near the compositional trend of the majority of komatiites from other regions (Fig. 3c).

With respect to FeO* content and Mg#, the komatiites of the Kostamuksha structure (eastern Karelia) are similar to the compositions of komatiites from other greenstone structures of Karelia, except for two samples with high iron contents, FeO* > 13 wt %, and low Mg# (~0.65). In the diagram (Fig. 3b), the Kostamuksha komatiites form a less steep negative regression trend, which is identical to the peculiar evolutionary trend of the compositions of komatiites from eastern Finland

Table 1. Concentrations of major, trace, and rare earth elements in the komatiites of the Baltic shield

Compo-nent	Hautavaara			Hizovaara		Kamennoozero		Koikari		
	427-2	427-5	427-7	576-4	575-2	224	224/1	1	350-1b	41-1/2
SiO_2	45.49	46.82	45.98	43.85	45.51	45.82	45.58	46.91	48.91	46.91
TiO_2	0.35	0.35	0.39	0.35	0.18	0.3	0.28	0.35	0.31	0.35
Al_2O_3	7.02	6.9	7.79	6.08	5.62	7.73	6.98	4.72	6.52	5.72
FeO*	11.91	11.54	11.68	12.8	11.72	9.56	9.61	8.05	9.3	8.05
MnO	0.2	0.21	0.16	0.31	0.18	0.28	0.21	0.13	0.11	0.14
MgO	30.66	28.41	28.82	29.97	35.28	30.78	30.46	33.86	28.01	32.84
CaO	4.32	5.71	5.13	6.52	1.46	5.42	6.73	5.95	6.72	5.95
Na_2O	0.03	0.05	0.03	0.09	0.02	0.04	0.1	0.01	0.04	0.01
K_2O	0.01	0.02	0.01	0.02	0.01	0.08	0.04	0.01	0.01	0.01
Sc	18	18	20	25	14				26	
Cr	1955	2172	2170	2208	1310	2701.64	2230	110		2102
Ni	706	644	584	857	1450	1379.64	1561	1400		1102
Co	97	80	79	97	870	86	91		67	69
V	181	162	202	171	197	140	131		120	
Cu	6	4	5	37	3			2400	11	
Zn	52	52	44	44	12				67	
Ti						1811	1931			1712
Zr	4	6	8	3	1	13	15		6	26
Y	5	6	6	7	3	4	3		6	10
La	1.50	2.16	1.58	0.53		0.42	0.51	0.38	0.67	0.45
Ce	2.96	4.62	3.65	1.58	0.56	1.50	1.82	1.30	2.60	1.52
Pr	0.40	0.72	0.45	0.21	0.11	0.21	0.38	0.26	0.40	0.30
Nd	1.99	3.29	2.37	1.01	0.60	1.37	2.17	1.50	2.00	1.76
Sm	0.58	0.82	0.75	0.38	0.27	0.49	0.72	0.59	0.65	0.69
Eu	0.18	0.30	0.19	0.10	0.05	0.18	0.27	0.22	0.21	0.26
Gd	0.92	1.22	0.85	0.55	0.50	0.68	0.82	0.96	0.70	1.13
Tb						0.15	0.17	0.16	0.11	0.19
Dy	0.87	1.12	0.93	0.53	0.44	0.81	1.02	1.16	0.94	1.17
Ho						0.18	0.25	0.23	0.20	0.27
Er	0.58	0.67	0.55	0.39	0.29	0.45	0.71	0.68	0.59	0.80
Tm						0.07	0.11	0.10	0.09	
Yb	0.68	0.87	0.70	0.35	0.35	0.42	0.69	0.56	0.52	0.66
Lu	0.10	0.14	0.10	0.05	0.05	0.07	0.12	0.10	0.08	0.12
$(Ce/Sm)_N$	1.23	1.36	1.17	1.01	0.50	0.73	0.61	0.53	0.97	0.53
$(Gd/Yb)_N$	1.09	1.13	0.98	1.28	1.16	1.31	0.95	1.39	1.09	1.39
Eu/Eu*	0.75	0.91	0.73	0.56	0.42	0.98	1.07	0.89	0.95	0.90
ΣHREE	4.01	5.19	3.98	2.38	2.06	2.70	3.91	3.75	3.14	4.27

Table 1. (Contd.)

Compo-nent	Kostamuksha				Palaya Lamba		Sovdozero			Kerety	Ingozero	Kareka Tundra
	547-10	737-2	746	s-197B	275-10	275-2b	9m01	9m05-2b	9m08-3b	19/92	235-a/85	753/87
SiO_2	45.31	48.12	48.39	48.76	45.66	45.2	46.16	44.7	46.32	44.14	45.09	45.51
TiO_2	0.28	0.35	0.26	0.52	0.25	0.28	0.32	0.47	0.34	0.19	0.17	0.46
Al_2O_3	5.94	6.04	6.01	6.36	6.19	7.09	6.35	7.22	5.48	4.58	5.07	7.38
FeO*	11.73	10.14	10.79	13.39	11.84	11.26	9.81	11.48	11.51	14.2	13.49	13.68
MnO	0.27	0.14	0.17	0.16	0.13	0.14	0.11	0.15	0.15	0.3	0.23	0.17
MgO	34.48	29.4	27.67	25.11	31.1	32.27	33.4	30.67	30.06	32.4	30.76	26.43
CaO	1.87	5.62	6.34	5.57	4.77	3.72	3.51	5.19	6.08	4.09	5.12	6.01
Na_2O	0.08	0.14	0.32	0.1	0.04	0.03	0.34	0.09	0.04	0.06	0.06	0.29
K_2O	0.03	0.04	0.04	0.01	0.01	0.01	0.01	0.04	0.01	0.04	0.02	0.04
Sc				29		23	21	33	24			
Cr					4492		2252	1965		3874	3981	3940
Ni				988	1310		1402			1654	1338	782
Co				92	94	89	90	90	86	147		99
V				176								
Cu				44								
Zn				72								
Ti					1141							2366
Zr				6	19	6	3	6	4	15	14	27
Y				10	7	4	5	7	6	5	5	9
La				1.60	1.30	1.20				1.61	0.22	0.47
Ce	0.97	1.32	1.84	3.50	2.80	2.10	2.32	2.30	2.60	3.55	0.82	1.15
Pr	0.12	0.26	0.22	0.60	0.35	0.30	0.35	0.38	0.40			
Nd	0.78	1.04	1.03	2.80	1.91	1.30	1.53	1.80	1.90	3.27	0.87	0.75
Sm	0.32	0.43	0.43	1.03	0.53	0.40	0.53	0.62	0.61	0.97	0.21	0.30
Eu	0.08	0.02	0.02	0.31	0.12	0.09	0.18	0.21	0.24	0.26	0.09	0.09
Gd	0.28	0.96	0.39	1.07		0.48	0.54	0.79	0.83			
Tb	0.05	0.13	0.10	0.21	1.53	0.10	0.10	0.14	0.15	0.19	0.06	0.11
Dy	0.32	0.82	1.02	1.64		0.70	0.80	1.10	1.05			
Ho	0.08	0.19	0.20	0.36		0.15	0.18	0.26	0.22			
Er	0.26	0.50	0.61	0.94		0.46	0.53	0.74	0.62			
Tm	0.04	0.06		0.15	0.10	0.07						
Yb	0.27	0.58	0.68	0.93	0.60	0.43	0.60	0.67	0.59	0.40	0.19	0.37
Lu	0.03	0.09	0.07	0.14	0.10	0.07	0.10	0.11	0.10	0.04	0.03	0.05
$(Ce/Sm)_N$	0.73	0.74	1.06	0.82	1.28	1.27	1.06	0.90	1.03	0.56	0.94	0.93
$(Gd/Yb)_N$	0.84	1.34	0.46	0.93		0.90	0.73	0.95	1.14			
Eu/Eu*	0.81	0.09	0.15	0.90		0.63	1.03	0.91	1.03			
ΣHREE	1.31	3.10	2.99	5.33	4.04	2.44	2.95	3.84	3.50	1.55	0.86	1.55

Table 1. (Contd.)

Compo-nent	Korva Tundra	Polmos-Porosozero					Ura Guba				
	723/87	185-a	194	200	200-a	202	9019g	9016	9014c/1	9014a/2	9014a
SiO_2	45.77	41.75	43.16	42.53	43.56	48.3	44.06	44.71	43.75	44.17	44.7
TiO_2	0.55	0.23	0.28	0.28	0.26	0.41	0.53	0.21	0.19	0.26	0.23
Al_2O_3	6.3	2.89	3.75	4.08	4.38	5.43	5.04	6.1	4.79	5.78	4.67
FeO^*	12.99	19.64	18.4	14.97	14.28	13.59	14.65	12.33	13.54	14.16	14.57
MnO	0.12	0.16	0.31	0.11	0.17	0.22	0.3	0.24	0.26	0.3	0.36
MgO	29.91	32.96	31.77	35.51	33.97	23.35	30.37	29.94	31.6	27.48	29.49
CaO	4.31	2.34	2.24	2.29	3.15	8.06	4.96	6.38	5.78	7.7	5.83
Na_2O	0.01	0.02	0.03	0.11	0.1	0.55	0.07	0.07	0.07	0.13	0.13
K_2O	0.01	0.02	0.06	0.06	0.06	0.09	0.02	0.02	0.02	0.02	0.02
Sc		13					12				21
Cr	6608	2138	3882	3654	3927	347	1556	2949	1530	2893	2191
Ni	1349	1109	1351	1983	1877	845	2279	1621	1847	1570	1690
Co	101	122		138			104	102	84	94	95
V											
Cu											
Zn											
Ti	2610							1974	846	2144	
Zr	26	5	14	15	16	23	3	12	17	28	4
Y	7	3	5	5	7	9	2	6	9	10	7
La	0.87	1.29	0.17	0.16	0.58	0.37	0.70	0.75	1.25	0.81	1.04
Ce	2.48	2.36	0.69	0.45	1.57	1.10	1.83	1.90	3.00	2.11	2.57
Pr		0.33					0.26				0.38
Nd	1.81	1.34	0.51	0.35	0.94	0.71	1.04	1.43	1.90	1.52	1.88
Sm	0.54	0.38	0.16	0.11	0.30	0.26	0.32	0.53	0.56	0.49	0.59
Eu	0.18	0.08	0.08	0.04	0.15	0.08	0.08	0.18	0.16	0.14	0.19
Gd		0.29					0.27				0.62
Tb	0.14	0.06	0.06	0.02	0.10	0.06	0.05	0.13	0.11	0.09	0.11
Dy		0.40					0.39				0.63
Ho							0.08				0.13
Er		0.25					0.23				0.34
Tm		0.03					0.03				0.05
Yb	0.47	0.23	0.22	0.07	0.31	0.26	0.18	0.52	0.49	0.35	0.32
Lu	0.07	0.04	0.04	0.01	0.04	0.03	0.03	0.08	0.080	0.05	0.05
$(Ce/Sm)_N$	1.11	1.50	1.06	0.99	1.25	1.01	1.38	0.87	1.29	1.04	1.05
$(Gd/Yb)_N$		1.02	1.05*	1.48*	1.32*	1.1*	1.21				1.55
Eu/Eu^*		0.73					0.83				0.98
$\Sigma HREE$	2.05	1.30	1.03	0.33	1.31	1.02	1.18	2.28	2.20	1.49	2.41

Note: $\Sigma HREE$ is the average total chondrite-normalized content of heavy lanthanides. $Eu/Eu^* = Eu_N / \sqrt{[(Sm)_N \cdot (Gd)_N]}$.

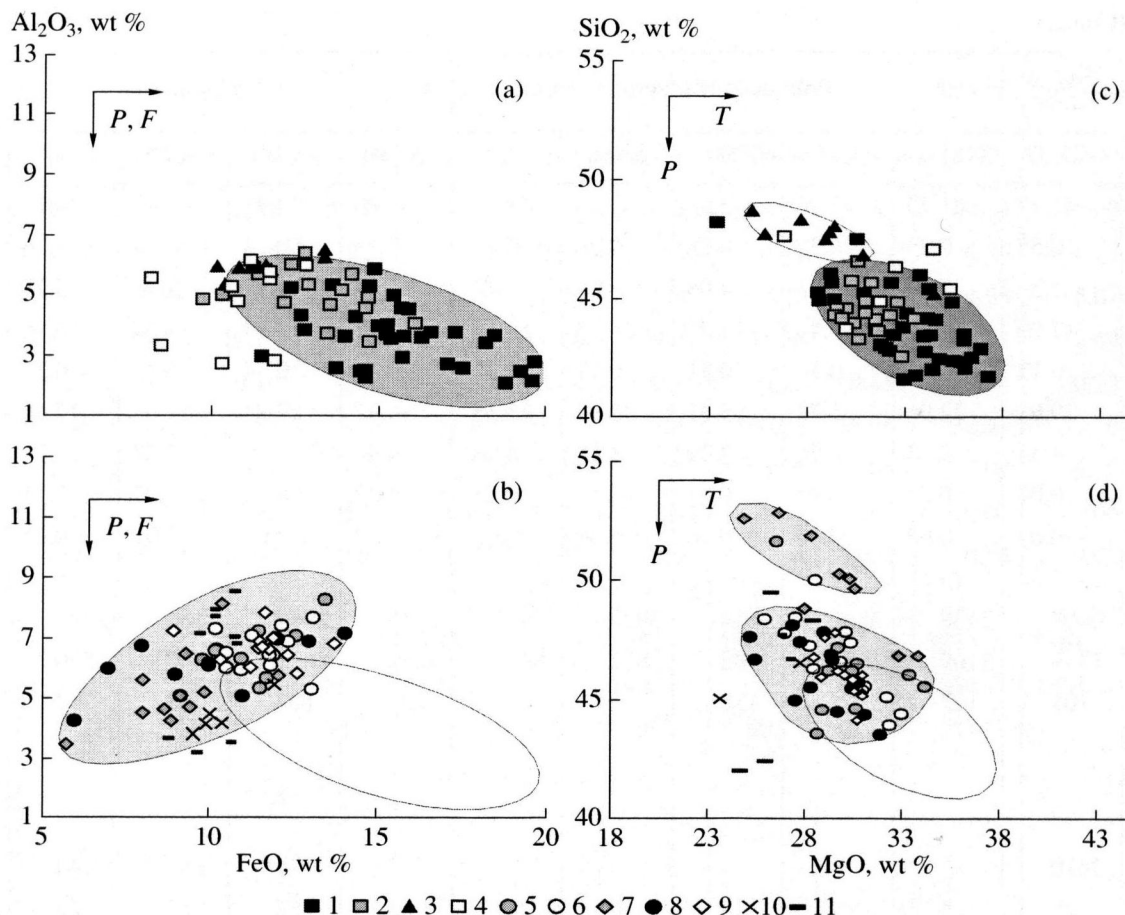* The value $(Gd/Yb)_N$ is extrapolated from Tb content.

Fig. 4. Variation diagrams (a), (b) Al_2O_3–FeO* and (c), (d) MgO–SiO_2 for the komatiites of the Baltic shield. Greenstone structures: (1) Polmos-Porosozero; (2) Ura Guba; (3) Kostamuksha; (4) Hizovaara; (5) Sovdozero; (6) Palaya Lamba; (7) Koikari; (8) Kamennoozero; (9) Hautavaara; (10) Ilomantsi; and (11) Kuhmo–Tipasjarvi. Arrows show directions of an increase in pressure (*P*), temperature (*T*), and degree of melting (*F*) according to experimental data (Hirose and Kushiro, 1993; Tronnes *et al.*, 1992; Wei *et al.*, 1990). The unshaded fields in Figs. 4b and 4d correspond to those in Figs. 4a and 4c.

(Kuhmo–Tipasjarvi–Ilomantsi belt) (Fig. 3c). This trend is conspicuous in a wide Mg# range (0.65–0.83) at very moderate variations in FeO* contents (10–11 wt %).

In the Al_2O_3–FeO* diagram (Figs. 4a, 4b), the komatiites of the Kola Peninsula and some komatiites of the Hizovaara structure (northern Karelia) form a compact field with low alumina (1.5–5.5 wt %) and high iron contents (FeO* = 12–18 wt %) (Fig. 4b). With respect to Al_2O_3 content, the komatiites of this group are comparable only to samples from the Koikari structure (Al_2O_3 = 3–6 wt %). The latter form together with the compositions of komatiites from the Kamennoozero structure of eastern Karelia a separate field, which is additionally distinguished by very low FeO* content (5–10 wt %) (Fig. 4a). On the whole, the compositions of central Karelian komatiites (Vedlozero–Segozero greenstone belt) are the most aluminous (Al_2O_3 = 5.5–8.0 wt %).

In the SiO_2–MgO diagram (Figs. 4c, 4d), the compositions of komatiites from the Kola Peninsula and northern Karelia, which are most magnesian (MgO =

28–38 wt %) and least siliceous (SiO_2 = 41–46 wt %), are distinctly different from the komatiites of the Koikari structure, which show the highest silica contents (up to 53 wt %). All other Karelian komatiites occupy a transitional position in this diagram (Fig. 4c).

Differences in the alumina contents of the Baltic shield komatiites are manifested in two general trends on the Al_2O_3–TiO_2 diagram (Figs. 5a, 5b):

—Al_2O_3/TiO_2 = 10–18, komatiites of the Kola Peninsula and northern Karelia; and

—Al_2O_3/TiO_2 = 18–23, komatiites of central Karelia except for some samples from the Koikari structure.

These two trends formed by the Baltic shield komatiites bear slight resemblance to the distinct trends of the compositions of Al-depleted ($Al_2O_3/TiO_2 \sim 10$) and Al-undepleted ($Al_2O_3/TiO_2 \sim 20$) komatiites from various regions (Fig. 5c).

In the Ti–Zr diagram (Figs. 6c, 6d) with the trends of chemical evolution for the derivatives of various types of modern mantle reservoirs (EM, enriched mantle; PM,
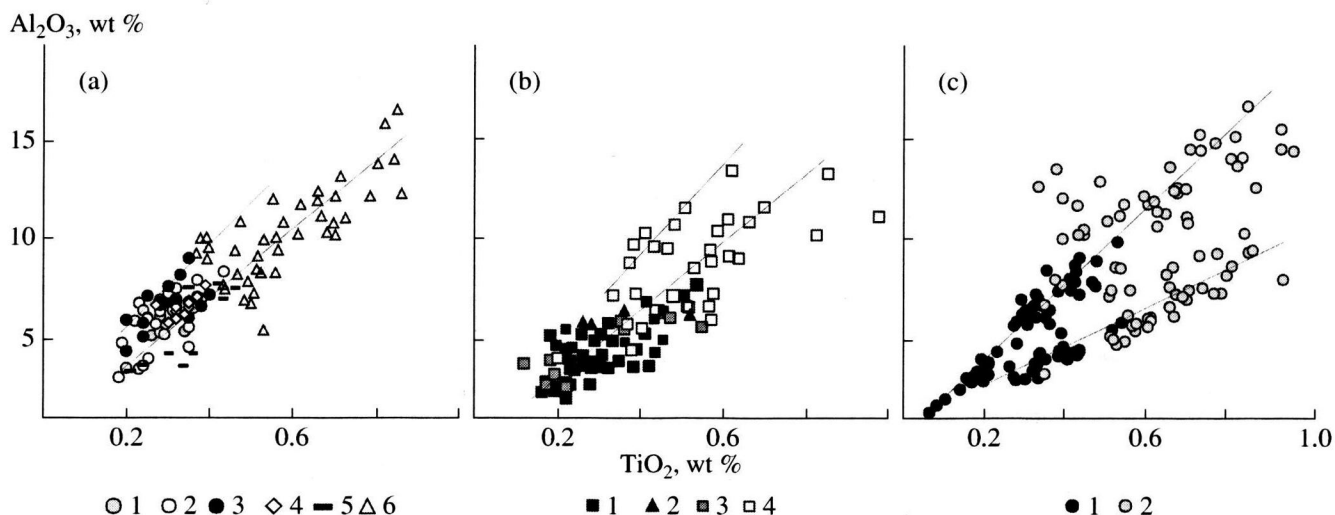
Al$_2$O$_3$, wt %

TiO$_2$, wt %

Fig. 5. Variation diagram Al$_2$O$_3$–TiO$_2$ for the komatiites of (a) central Karelia, eastern Karelia, and eastern Finland; (b) the Kola Peninsula, northern Karelia, and western Karelia; and (c) other world regions. (a) (1) Sovdozero; (2) Koikari and Palaya Lamba; (3) Kamennoozero; (4) Hautavaara structures; (5) eastern Finland; and (6) komatiitic basalts of central and eastern Karelia. (b) (1) Polmos-Porosozero and Ura Guba structures; (2) Kostamuksha structure; (3) Hizovaara structure; and (4) komatiitic basalts of the Kola Peninsula. (c) (1) Komatiites and (2) komatiitic basalts from other regions.

primitive mantle; and DM, depleted mantle), almost all compositions of komatiites from the Kola Peninsula, northern Karelia, and western Karelia plot along the primitive mantle trend (Fig. 6c). The Karelian komatiites show more considerable Ti/Zr variations. The compositions of komatiites from eastern Karelia (Kamennoozero structure) form a separate field along the evolutionary trend of the depleted mantle (DM), whereas the majority of komatiites from central Karelia (Vedlozero–Segozero greenstone belt) show lower Ti/Zr values approaching the enriched mantle trend (EM). Exceptions are some komatiites from the Koikari and Sovdozero structures with Ti/Zr values approaching the primitive mantle (CHUR) trend and low initial Nd isotopic ratios.

Variations in the Y/Zr ratio (Figs. 6a, 6b) of komatiites from various greenstone belts of the Baltic shield correspond to the trends in the Ti–Zr coordinates. Exceptions are some komatiite samples from the Hautavaara structure showing Y/Zr ratios much lower than that of the primitive mantle, which is also reflected in the Nd isotopic composition of these samples.

Rare Earth Elements (REE)

The komatiites of the Baltic shield represented by samples of spinifex zones and flowtop breccias can be divided into three groups with respect to the chondrite-normalized (McDonough and Sun, 1995) distribution of light lanthanides (LREE) (Fig. 7):

type I, chondrite (flat) REE distribution [(Ce/Yb)$_N$ = 0.8–1.2] is characteristic of the komatiites of the Polmos-Porosozero, Ura Guba, Palaya Lamba, Sovdozero, and Kostamuksha structures;

type II, depleted to varying degrees in LREE [(Ce/Sm)$_N$ = 0.61–0.7 and (Ce/Yb)$_N$ = 0.4–0.9] komatiites of the Polmos-Porosozero, Hizovaara, Koikari, Kamennoozero, and Tipasjarvi structures; and

type III, LREE-enriched [(Ce/Sm)$_N$ = 1.5 and (Ce/Yb)$_N$ = 1.3–1.5] and HREE unfractionated distribution patterns [(Gd/Yb)$_N$ = 0.8–1.0] detected in the komatiites of the Hautavaara and Suomussalmi structures.

In addition to the different distribution patterns and contents of LREE, the komatiites display considerable variations in the average total chondrite-normalized contents of HREE (ΣHREE$_N$ = 0.3–0.6) at similar Mg# values (0.63–0.78) (Fig. 7). The following three groups of komatiites can be distinguished on the basis of chondrite-normalized HREE abundances (ΣHREE$_N$). Each of these groups comprises all geochemical LREE types (Fig. 7).

Group I (0.3–2.5 chondr.):

Ia (0.3–1.5 chondr.), Kola Peninsula (Polmos-Porosozero and Ura Guba structures), part of eastern Finland (Ilomantsi structure), and western Karelia (Kostamuksha structure);

Ib (1.9–2.5 chondr.), Kola Peninsula (Polmos-Porosozero, Ura Guba, and Korva Tundra structures), northern Karelia (Hizovaara and Kerety structures), and part of eastern Finland (Kuhmo).

Group II (2.5–4.5 chondr.), eastern Karelia (Kamennoozero structure) and central Karelia (Koikari, Palaya Lamba, Sovdozero, and Hautavaara structures).
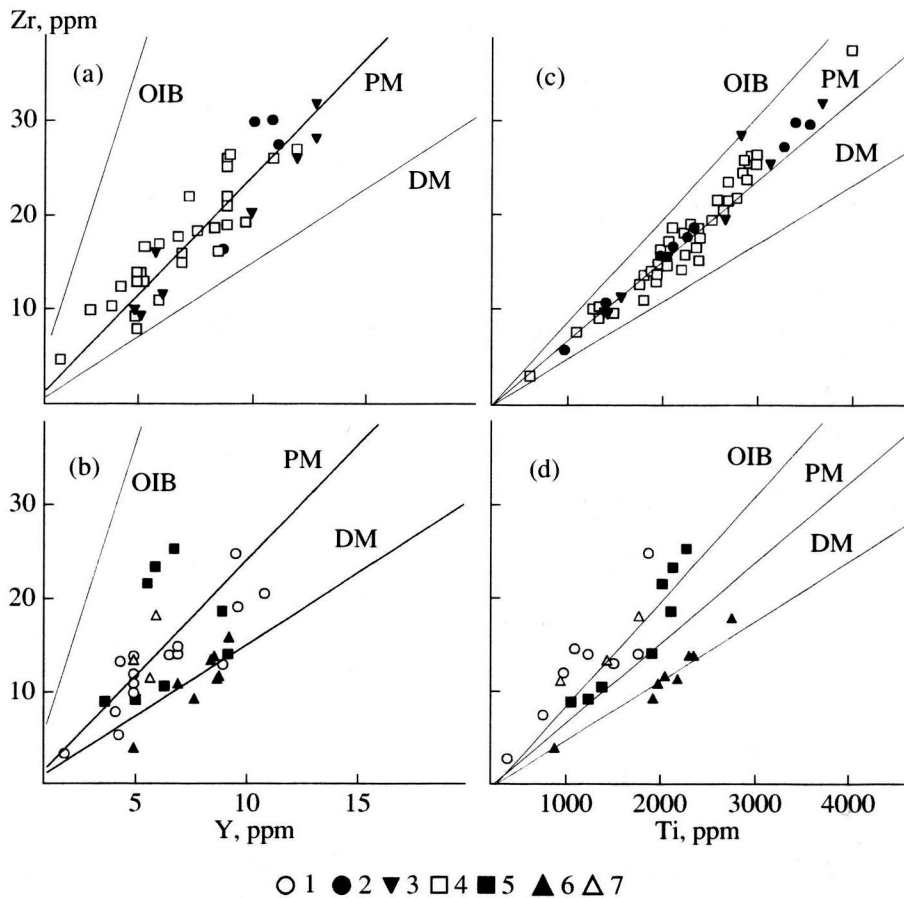
Fig. 6. Relations of Ti, Y, and Zr contents in the komatiites of (b), (d) central and eastern Karelia and (a), (c) the Kola Peninsula, northern Karelia, and westerns Karelia. Greenstone structures: (1) Palaya Lamba and Koikari; (2) Kostamuksha; (3) Hizovaara; (4) Kola Peninsula; (5) Sovdozero; (6) Kamennoozero; and (7) Hautavaara.

Group III (4.5–6.5 chondr.), eastern Finland (Kuhmo–Suomussalmi structure) and part of western Karelia (Kostamuksha structure).

ESTIMATION OF THE TEMPERATURES AND PRESSURES OF KOMATIITE FORMATION

A comparison of the data on the chemical heterogeneity of komatiites from the Baltic shield with the results of experimental studies on the melting of Tinaquillo lherzolite, garnet lherzolite KLB-1, spinel lherzolite HK-66 (Hirose and Kushiro, 1993), and komatiites (Wei *et al.*, 1990) (Fig. 8) allowed us to conclude that the komatiites of the Kola Peninsula and northern Karelia were derived at relatively high temperatures and great depths as compared with the komatiites of central and eastern Karelia, which is in agreement with the resemblance of their Ti/Zr trend to that of the primitive mantle (PM).

Extrapolation of the experimental points on the melting of spinel lherzolite HK-66 yielded the following empirical dependency of the depth of mantle melt generation on silica content (Scarrow and Cox, 1995):

$$P(\text{kbar}) = 213.6 - 4.05\text{SiO}_2.$$

The theoretical calculations of the conditions of komatiitic melt generation by A.V. Girnis and I.D. Ryabchikov (*Komatiity i...*, 1988) also suggested that an increase in pressure reduces the cation fraction of Si in the melt in equilibrium with olivine and orthopyroxene.

The application of these dependencies and calculations to the estimation of the relative depths of generation of komatiitic melts from the Baltic shield (Fig. 9a) allows us to conclude that the komatiites of the Kola Peninsula and northern Karelia were derived at greatest depths, and the komatiites of the Palaya Lamba structure show the lowest pressure of generation among the relatively shallow komatiites of Karelia.

The liquidus temperature of komatiite magmas can be estimated from the experimentally calibrated dependency of melt temperature on the concentration of MgO (Nesbet *et al.*, 1993):

$$T_m = 1400°C + 20(\text{MgO, wt \%} - 20).$$

In these calculations, the concentrations of MgO (wt %) in initial melts were estimated from the analyses of komatiites from spinifex and flowtop breccia zones.
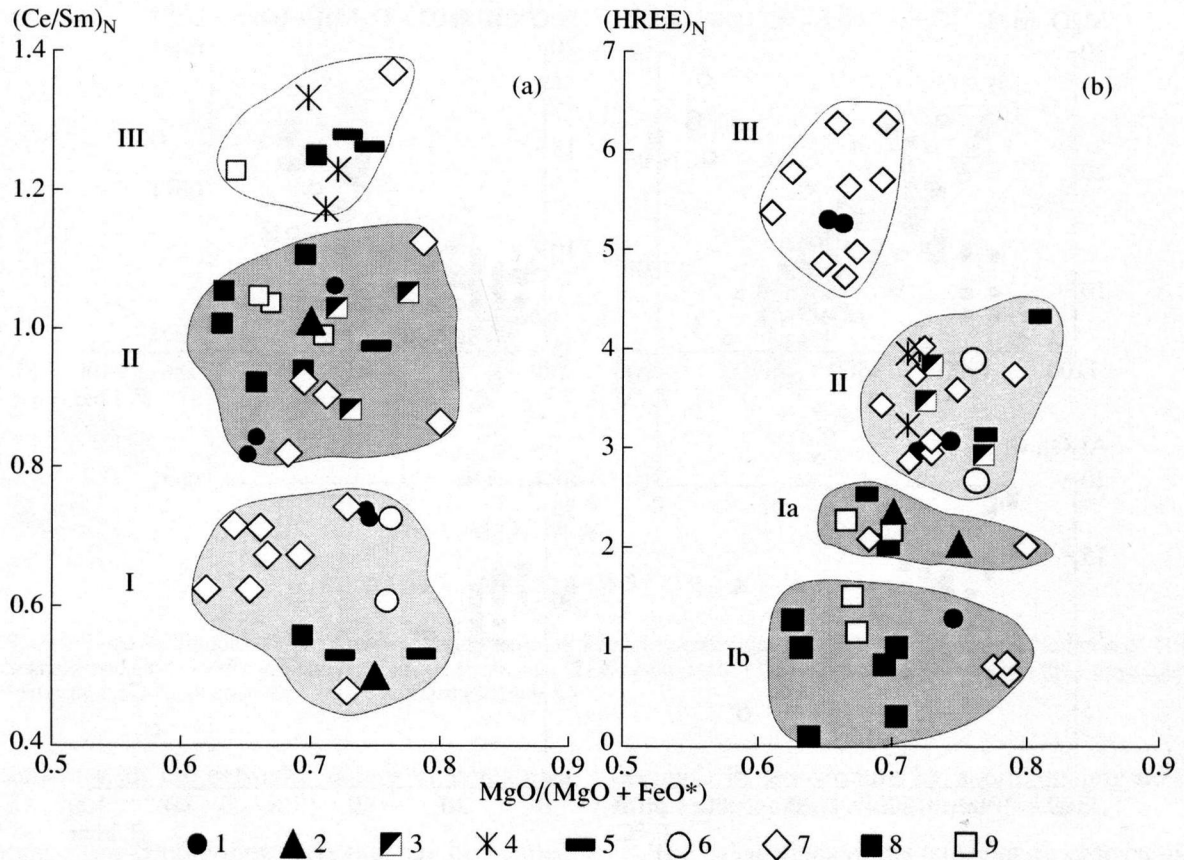
Fig. 7. Geochemical (a) types and (b) groups of komatiites of the Baltic shield discriminated with respect to the distribution and contents of light and heavy lanthanides as functions of MgO/(MgO + FeO*). Structures: (1) Kostamuksha; (2) Hizovaara; (3) Sovdozero; (4) Hautavaara; (5) Palaya Lamba and Koikari; (6) Kamennoozero; (7) Kuhmo–Suomussalmi; (8) Polmos-Porosozero; and (9) Ura Guba.

The calculation of melt eruption temperatures using the average compositions of komatiites, the compositions of spinifex-textured komatiite zones, and all compositions of komatiites from the Baltic shield revealed some general tendencies in the temperatures of komatiite melts, which are in agreement with experimental data (Figs. 8, 9). There are direct experimental data on the melting of Archean komatiites (Girnis *et al.*, 1987; Green, 1981; *Komattity i...*, 1988; Wei *et al.*, 1990), which demonstrated that the temperatures of erupted komatiites were as high as 1600–1650°C. The high temperatures of the peridotitic komatiite melts are reflected in their mineralogical characteristics. Their major minerals are highly magnesian olivine (Fo_{86-94}), clinopyroxene often with high alumina contents (up to 6–8 wt %), chrome spinel, and magnetite. The experimental investigation of olivine in equilibrium with komatiite melt under various $P-T$ conditions demonstrated that its composition changes from $Fo_{89.4}$ at $P = 4$ GPa and $T = 1700$°C to Fo_{92} at $P = 7$ GPa and $T = 1830$°C (Tronnes *et al.*, 1992).

Spinifex olivine from the komatiites of the Baltic shield (Table 2) shows high Mg# values (Fo_{89-90}) and is almost nickel-free. The low content of NiO in olivine

from the chill zones of peridotitic komatiite lavas can be explained on the basis of experimental evidence on the melting of synthetic nickel and magnesium olivines, which form continuous solid solutions (Velinskii and Bannikov, 1986; Hatton, 1984). The melting temperatures of synthetic olivines from these experiments (1890°C for Mg_2SiO_4 and 1670°C for Ni_2SiO_4) are much higher that the liquidus temperature of komatiite. However, addition of 10% fayalite depresses the melting temperature of olivine (Fo_{90}) to 1650°C, which is close to the eruption temperature of peridotitic komatiites. The low Ni content of the spinifex olivine could be related to the crystal chemical features of its occurrence, which is controlled by the predominant growth along the c axis with the maximum reticular density of the structure. There is a direct correlation between the distribution coefficients of cations in the olivine structure (KD = MgM1 × NiM2/MgM2 × NiM1) among the M1 and M2 positions in cation–oxygen octahedra (C–O) and temperature, which is related to the preferential partitioning of Ni into the M1 position. In the case of spinifex olivine crystallization at high temperature, the chain structure of C–O octahedra is distorted, and the resulting values of the energy potential of the
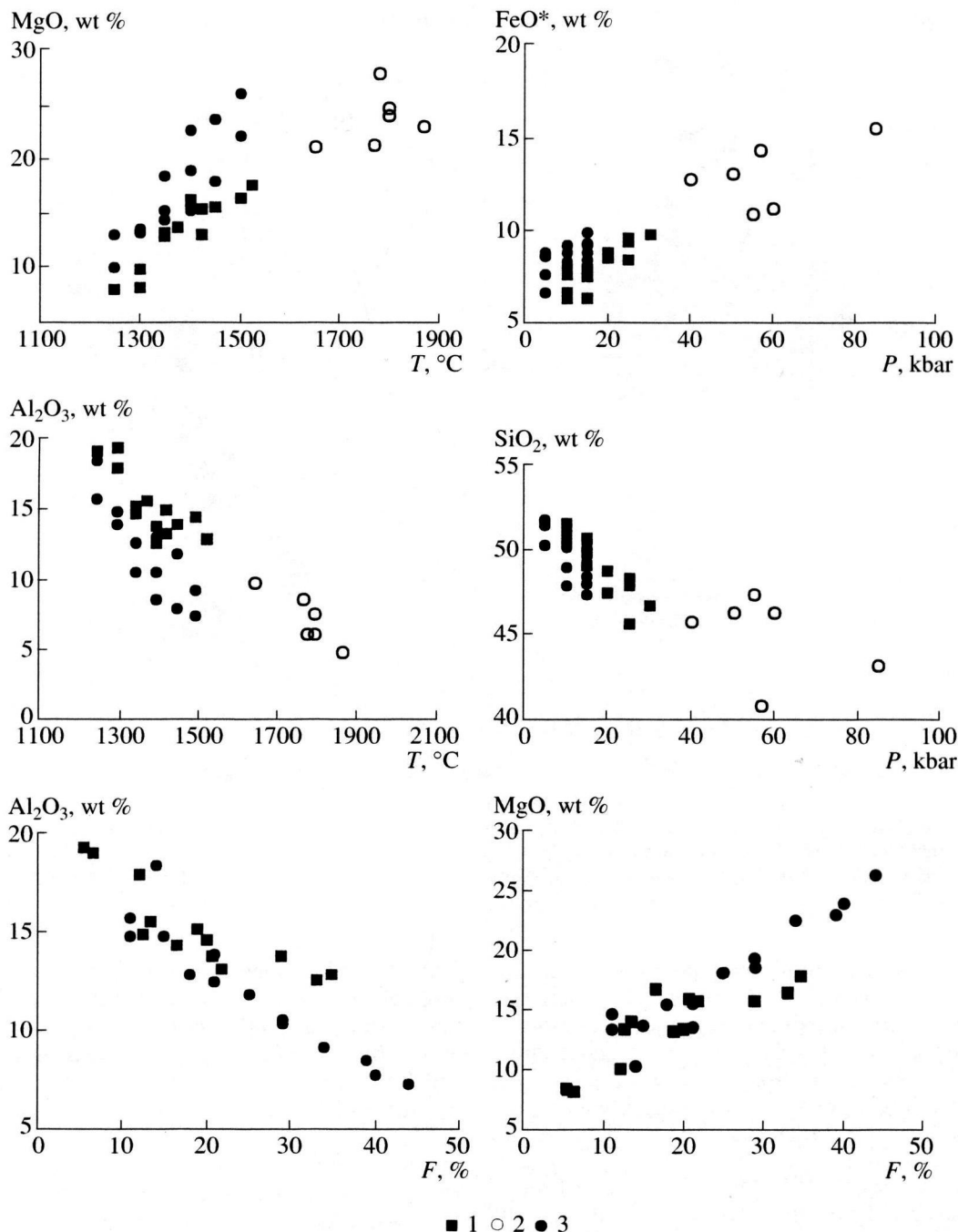
Fig. 8. Variations in the concentrations of MgO, FeO*, Al$_2$O$_3$, and SiO$_2$ in experimental melts produced by melting of (1) lherzolite KLB-1, (2) AUK komatiite, and (3) Tinaquillo lherzolite under varying parameters (*P*, *T*, and *F*) (Hirose and Kushiro, 1993; Tronnes *et al.*, 1992).

internal crystal field prevent the incorporation of cations with electronegativity higher than that of Mg^{2+} in the M1 position (Ganguli, 1977; Hart, 1978). The occurrence of NiO (0.19 wt %) in the composition of olivine with a normal habit from the cumulative peridotitic komatiites suggests that this mineral crystallized at lower temperature, which agrees with the probable temperature distribution during komatiite flow solidification.

A characteristic feature of olivine from komatiites is its high calcium content (up to 0.28 wt %). A CaO content of 0.1 wt % is the boundary value between the compositions of olivines from ultrabasic extrusive rocks (CaO > 0.1 wt %) and ultrabasic deep-seated plutonic rocks (CaO < 0.1 wt %) (Ryabov, 1992). An increase in calcium content in olivine from komatiite is possible at a significant pressure decrease and constant or slightly decreasing temperature of its crystallization, which is

$T°$, C = 1400 + [(MgO – 20) × 20]

P, kbar = 213.6 – 4.05P × SiO$_2$
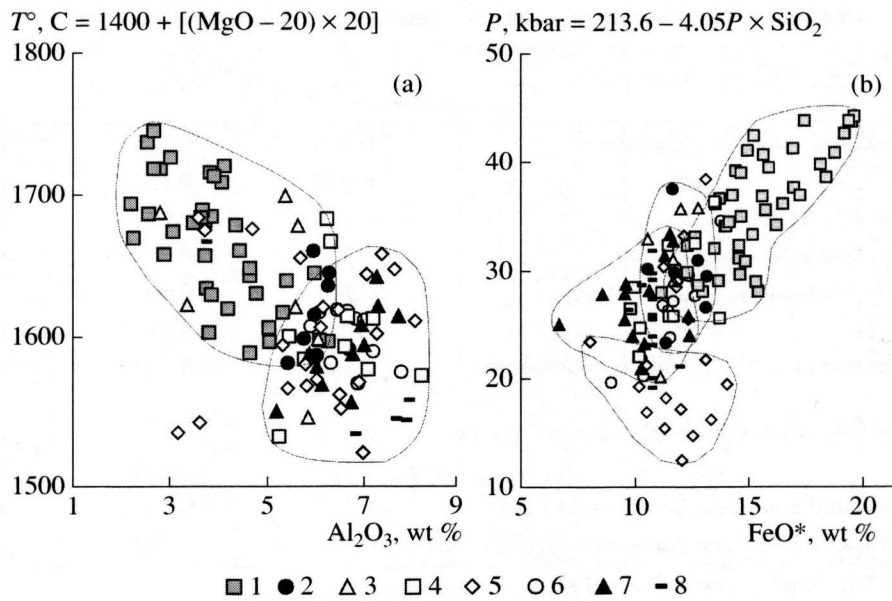
Fig. 9. Calculated (a) liquidus temperatures and (b) pressures of komatiite generation for the Baltic shield after Nesbet *et al.* (1993) and Scarrow and Cox (1995). Structures: (1) Kola Peninsula; (2) Kostamuksha; (3) Hizovaara; (4) Sovdozero; (5) Palaya Lamba; (6) Hautavaara; (7) Kamennoozero; and (8) eastern Finland.

in agreement with the extrusive nature of komatiites (Table 3).

Among a few geothermometers that can be applied to high-temperature komatiites, which are almost free of primary minerals, are those based on the dependency of the fayalite mole fraction of olivine on the composition of the parental melt and equilibrium temperature in "dry" systems at atmospheric pressure (Vaganov and Sokolov, 1988). A comparison of the calculated temperatures of komatiite liquidus with experimental data shows their consistency within ±50°C and a regular

decrease in temperature by approximately 60–100°C from top to bottom within flows (Table 3).

The calculations of the temperature characteristics of komatiites and their mantle sources suggest at least over-heating of the mantle sources of the Baltic shield komatiites as compared to the temperature of the surrounding mantle according to the Richter (1988) model and considerable variations in the thermodynamic parameters of their petrogenesis, which cannot be explained within the models of chemically and thermally homogeneous convecting mantle (Vrevsky *et al.*, 1996; Dobretsov *et al.*, 2001).

Table 2. Compositions of olivine from the komatiites of the greenstone belts of the Baltic shield

Oxide	1	2	3	4	5	6	7	8	9	10
	189	189a	245a	245b	207	203	235a	224	9014	
SiO$_2$	42.17	42.16	40.80	40.74	40.25	37.62	38.79	41.98	40.52	39.07
FeO	9.85	10.09	8.31	7.68	10.84	26.43	19.52	9.76	11.04	14.61
MnO	0.40	0.41	0.34	0.46	0.27	0.33	0.25	0.53	0.41	0.08
MgO	48.11	47.10	49.69	50.13	47.56	35.68	41.76	47.46	48.13	44.79
CaO	0.28	0.24	0.28	0.20	0.11	0.01	–	0.27	0.27	–
CoO						0.04	0.02			–
NiO	–	–	0.21	0.17	–	0.23	0.26	–	–	0.58
Cr$_2$O$_3$	–	–	0.23	–	–	–	–	–	0.33	–
N	2	2	1	1	3	4	4	3	2	1

Note: (1)–(5) Polmos-Porosozero structure: (1), (2), and (5) spinifex zone A1 and (3)–(4) cumulative zone B1; (6) Imandra structure; (7) Tersk structure, pyroxenite komatiite with pillow structure; (8) Kamennoozero structure, spinifex zone A1; (9)–(10) Ura Guba structure, (9) spinifex and (10) cumulative zones. Samples (1)–(8) were analyzed on ARL (Karpinskii All-Russia Research Institute of Geology) and CAMECA electron microprobes (Geological Institute, Kola Research Center, Russian Academy of Sciences); and (9) and (10) are after Smolkin (1992).

Table 3. Liquidus temperatures of komatiites calculated after Vaganov and Sokolov (1988)

Sample no.	Rock, texture (reference)	$\log X_{Ol}^{liq}$	$Fe^{2+}/(Fe^{2+} + Mg)^{liq}$	$T°, C_{calc}$	$T°, C_{exp}$
SF-134	Spinifex-textured komatiite, Belingwe[1]	0.104	0.158	1671	–
B-4	Same	0.083	0.167	1690	–
SA-2048	Same, zone A1, Abitibi[2]	0.089	0.214	1670	1510
SA-2039	Cumulative komatiite (B2), Abitibi	0.128	0.229	1620	1610
J-49	Spinifex-textured komatiite, Barberton[3]	0.079	0.090	1740	1730
J-49	Same	0.083	0.138	1710	1700
189	Spinifex-textured komatiite, Polmos-Porosozero structure	0.116	0.242	1610	–
245-a	Cumulative komatiite, Polmos-Porosozero structure	0.136	0.230	1590	–
245-b	Same	0.132	0.196	1640	–
9014	Spinifex-textured komatiite, Ura Guba structure	0.105	0.218	1665	–
224	Spinifex-textured komatiite, Kamennoozero structure	0.139	0.212	1595	–

Note: [1] Nesbet *et al.* (1977); [2] Arndt (1994); [3] Green (1981).

ND ISOTOPIC SYSTEMATICS AND AGE OF KOMATIITES

In order to refine the obtained characteristics and extend our knowledge of the petrochemical and geochemical differences among the Archean komatiites of the Baltic shield, their primary melts, and mantle sources, their Nd isotopic characteristics were investigated. These investigations aimed at determining relationships between variations in the compositions of komatiites and the isotopic geochemical heterogeneity of mantle sources of their primary melts. In addition, we attempted to obtain independent geochronological information on the timing of separation of the mantle sources of komatiites of various geochemical types.

The results of these investigations demonstrated that the initial $^{143}Nd/^{144}Nd$ ratios and, correspondingly, $\epsilon Nd(T)$ values show significant variations in the Baltic shield komatiites (Table 4).

In general, mantle-derived igneous rocks, including obviously komatiites, may show variations in the initial $^{143}Nd/^{144}Nd$ ratio relative to the isotopic evolution path of depleted mantle (DePaolo and Wasserburg, 1976) owing to the following factors: (a) heterogeneity of mantle sources including a specific evolution of mantle isotopic signatures different from that accepted in the model of DePaolo and Wasserburg (1976); (b) contamination of mantle melts with crustal material; and (c) analytical errors ($>2\sigma$).

Taking into account the above-described constraints, the Baltic shield komatiites can be divided into three main groups similar to the derivatives of some modern isotopic types of mantle reservoirs:

(1) DM_1, "normal" depleted mantle;

(2) DM_2, "strongly" depleted mantle; and

(3) UM and EM, undepleted and enriched mantle.

Type DM_1. The komatiites of the Kola Peninsula (Polmos-Porosozero and Ura Guba structures) and Hizovaara and Kostamuksha greenstone structures of Karelia (Table 4) belonging to the second age group show an average value of $\epsilon Nd(T = 2870) = +2.5$. In the Sm–Nd evolution diagram, they spread around the regression line with a slope corresponding to an age of 2860 ± 92 Ma and $\epsilon Nd = +2.6 \pm 0.3$ (MSWD = 0.84, Fig. 10). This correlation can be interpreted as either a mixing line between the derivatives of isotopically different mantle reservoirs or a mantle isochron, whose slope is controlled by the time of mantle source separation. Since the processes of source mixing as well as crustal contamination usually give rise to an increase in Sm–Nd model age, and the observed correlation corresponds within errors to the U–Pb isochron age of volcanism in these structures (Fig. 2), this dependency probably reflects the generation of the komatiites from a single mantle reservoir with $\epsilon Nd = +2.6 \pm 0.3$. In addition, the absence of a correlation between Nd isotopic composition and 1/Nd (Fig. 17) in komatiite samples from the Kola Peninsula (Polmos-Porosozero and Ura Guba structures) and Hizovaara and Kostamuksha greenstone structures of Karelia also supports the reliability of the isochron age and homogeneous mixing of materials from various mantle sources.

The existence of a common isotopic mantle reservoir for the komatiites of the Kola Peninsula, northern Karelia, and part of eastern Karelia is additionally supported by the fact that 12 komatiite samples from the Polmos-Porosozero, Korva Tundra, and Ura Guba structures (Table 4) form a regression line with a slope corresponding to an age of 2882 ± 190 Ma, $\epsilon Nd = +2.8$, and MSWD = 3.9 (Fig. 11), and 15 komatiite and basalt samples from the Kostamuksha structure (Table 4) define an isochron with an age of 2889 ± 100 Ma, $\epsilon Nd = +2.2$, and MSWD = 0.77 (Fig. 12). The data

Table 4. Sm–Nd data for the komatiites and tholeiitic basalts of the Archean greenstone belts of the Baltic shield

No.	Sample	Sm, ppm	Nd, ppm	$^{147}Sm/^{144}Nd$	$^{143}Nd/^{144}Nd$	εNd(2879)	±2σ
			Ura Guba structure				
1	9022a	1.970	5.40	0.22071	0.51317	+1.6	13
2	9016	0.626	1.67	0.22670	0.51334	+2.6	14
3	9012	2.740	8.11	0.20440	0.51288	+1.8	17
4	6294	0.615	1.64	0.22970	0.51339	+2.5	13
5	9004	1.800	5.17	0.21137	0.51304	+3.3	16
6	9013a	0.702	1.95	0.21877	0.51316	+2.0	17
7	9015a	1.530	4.40	0.21136	0.513307	+3.0	12
8	14294	1.030	2.65	0.23630	0.51352	+2.7	12
9	14194	0.669	1.77	0.22858	0.51339	+2.8	16
			Polmos-Porosozero structure				
10	200	0.576	2.11	0.16580	0.51221	+3.2	10
11	200-a	0.509	1.74	0.1778	0.51245	+3.0	12
			Korva Tundra structure				
12	753	0.419	1.48	0.17130	0.512378	+3.7	3
			Hizovaara structure				
13	576-4	0.419	1.99	0.21990	0.51326	+3.6	15
			Kostamuksha structure				
			Komatiites				
14	737-2	1.250	3.240	0.23490	0.513500	+3.1	9
15	746	1.110	2.790	0.24190	0.513630	+3.1	8
16	15/197V	0.160	0.403	0.18119	0.512480	+2.5	19
17	15/292V	2.514	7.523	0.23690	0.513520	+2.8	11
18	11/93	1.589	4.370	0.21004	0.512990	+2.1	18
19	12/93	2.415	7.453	0.20256	0.512870	+2.4	22
20	109-lzh	0.995	2.300	0.26089	0.513990	+3.3	19
			Basalts				
21	8285-ar	0.520	1.323	0.23686	0.513490	+2.2	17
22	9085-ar	2.860	8.513	0.20258	0.512830	+1.6	22
23	3685-AR	1.304	3.863	0.20350	0.512830	+1.4	12
24	4485-AR	1.956	5.900	0.19999	0.512840	+2.8	15
25	2285-AR	1.265	3.698	0.20625	0.512900	+1.6	18
26	2585-AR	2.126	6.161	0.20812	0.512990	+2.7	22
27	82a85-ar	0.520	1.323	0.23686	0.513480	+2.0	20
28	118-LZh	1.856	5.356	0.20897	0.513015	+3.0	16
			Hautavaara structure				
29	427-2	0.613	1.989	0.18690	0.512530	+1.8	8
30	427-7	0.509	1.62	0.1906	0.512535	+0.4	41
			Palaya Lamba structure				
31	275-10	0.304	0.849	0.2171	0.513102	+1.3	13
32	5410-6	0.30	0.75	0.2449	0.513603	+0.6	21
33	60-8a	0.82	2.18	0.2268	0.513297	+1.5	13
34	60-9	0.83	2.16	0.2319	0.513340	+0.4	20
			Sovdozero structure				
35	9m01	0.467	1.27	0.22296	0.513312	+3.3	48
36	9m08-3	0.610	1.64	0.22536	0.51332	+2.5	65
37	9m18-1	0.950	2.52	0.22897	0.513336	+1.4	34
38	971	2.660	6.12	0.26368	0.514025	+1.7	13
			Koikari structure				
39	9-50	1.15	3.04	0.2291	0.513343	+1.5	10
40	350-61	0.87	2.33	0.2243	0.513256	+1.4	13
41	90-1	0.83	2.30	0.2176	0.513288	+4.7	12
42	2-1	0.78	2.02	0.2322	0.513424	+1.9	22
43	847-1	1.37	4.35	0.1898	0.512573	+1.4	11
44	849-1	1.64	5.20	0.1910	0.512624	+1.9	10
			Kamennoozero structure				
45	224/1	0.62	2.85	0.15670	0.512059	+3.8	11
46	224	0.765	2.835	0.16370	0.512214	+4.2	11

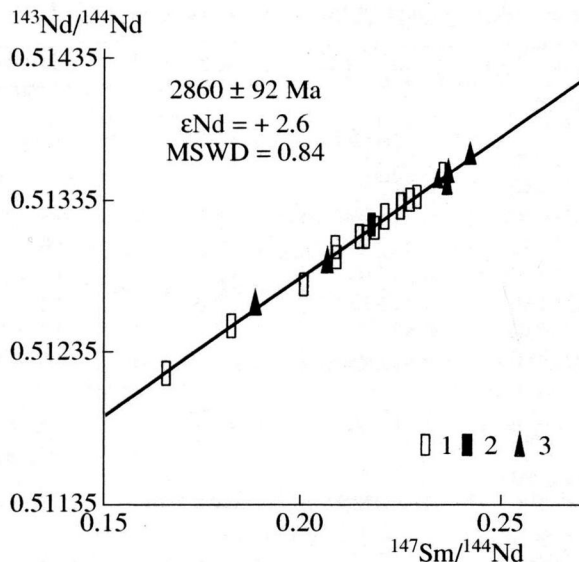Note: Sample nos. 32–34, and 38–44 are after Svetov and Huhma (1999).

Fig. 10. Sm–Nd evolution diagram for the komatiites of greenstone belts. (1) The Kola Peninsula (Polmos-Porosozero, Ura Guba, and Korva Tundra structures), (2) northern Karelia (Hizovaara structure), and (3) western Karelia (Kostamuksha structure).
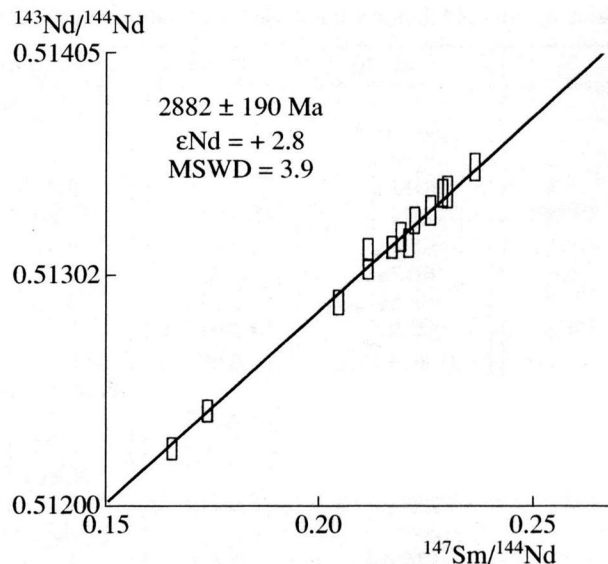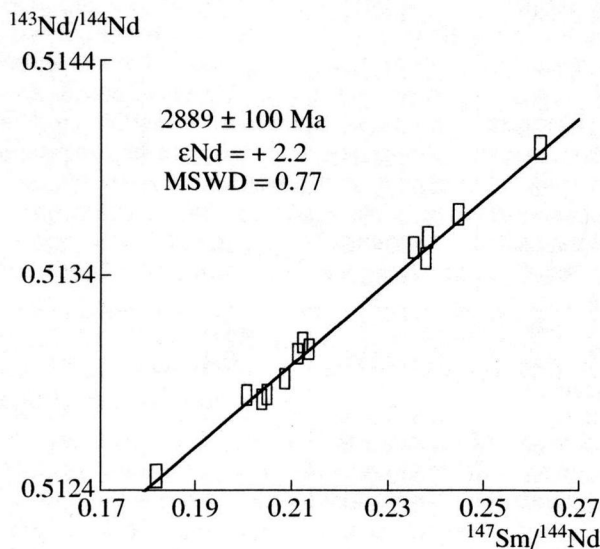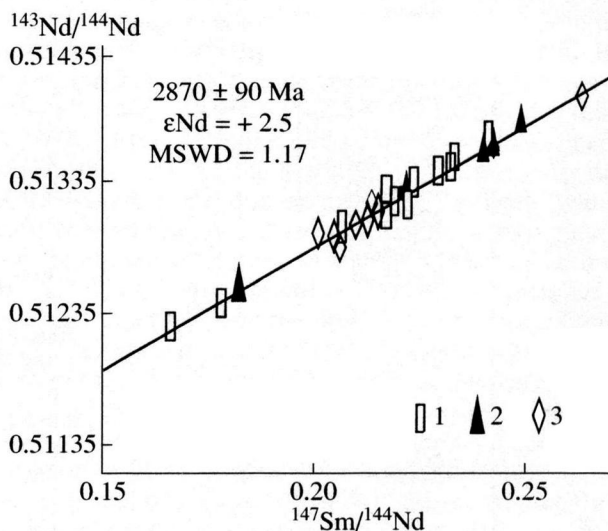

Fig. 11. Sm–Nd evolution diagram for the komatiites of the greenstone belts of the Kola Peninsula (Polmos-Porosozero, Ura Guba, and Korva Tundra structures).

Fig. 12. Sm–Nd evolution diagram for the komatiites and tholeiitic basalts of the Kostamuksha greenstone structure, western Karelia.

Fig. 13. Sm–Nd evolution diagram for the komatiites and tholeiitic basalts of greenstone belts. (1) The Kola Peninsula (Polmos-Porosozero, Ura Guba, and Korva Tundra structures), (2) northern Karelia (Hizovaara structure), and (3) western Karelia (Kostamuksha structure).

obtained for the Kostamuksha structure are comparable with a $^{206}Pb–^{204}Pb$ isochron age of 2771 ± 110 Ma for the komatiites and basalts and Sm–Nd isochron ages of 2843 ± 39 and 2798 ± 52 Ma for the komatiites and tholeiites (εNd from +2.9 to +3.4) (Puchtel *et al.*, 1998). The "regional" isochron constructed using all 28 komatiite and tholeiite samples from the Kola Peninsula (Polmos-Porosozero, Korva Tundra, and Ura

Guba structures) and the Hizovaara and Kostamuksha greenstone structures of Karelia (Table 4) yields practically the same age (2870 ± 90 Ma, εNd = 2.5, and MSWD = 1.17; Fig. 13).

The feasibility of regarding the komatiites of all these structures as derivatives of a uniform mantle reservoir is also suggested by their common deepest and highest temperature nature, geochemical similarity, and affiliation to
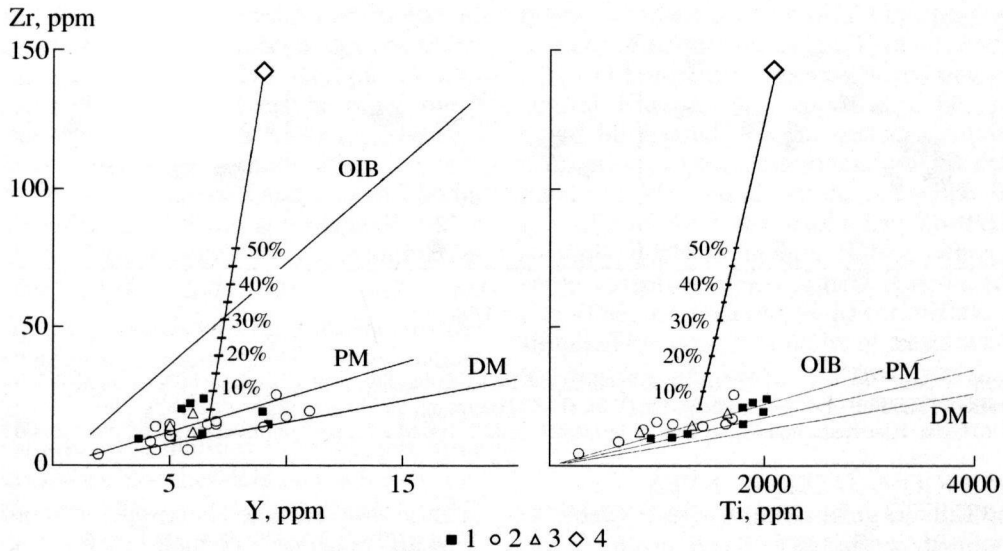
Fig. 14. Relations of Ti, Y, and Zr contents in the komatiites of the (1) Sovdozero, (2) Koikari, and (3) Palaya Lamba and Hautavaara structures, and (4) model trends of their crustal contamination. The average composition of old (>3.1 Ga) tonalites of the Vodlozero block (Lobach-Zhuchenko *et al.*, 1993) was used as the contaminant composition.
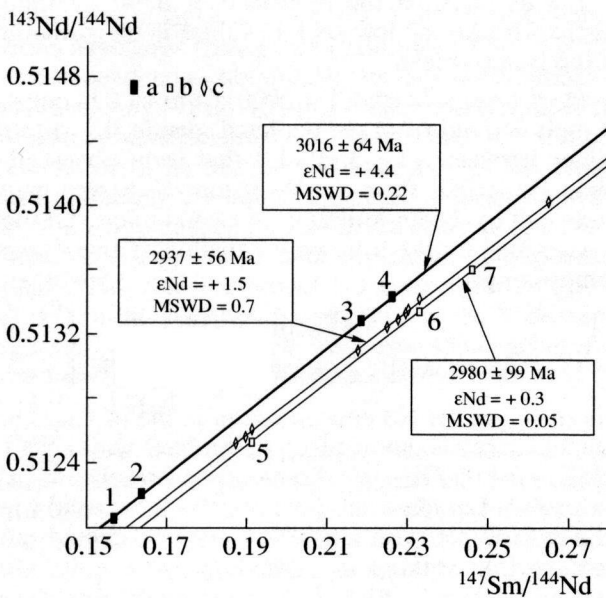

Fig. 15. Sm–Nd evolution diagram for the komatiites of central and eastern Karelia.

(a) (1), (2) Kamennoozero, (3) Sovdozero, and (4) Koikari structures.

(b) (5), (6) Palaya Lamba and (7) Hautavaara structures.

(c) Vedlozero–Segozero greenstone belt (Table 5).
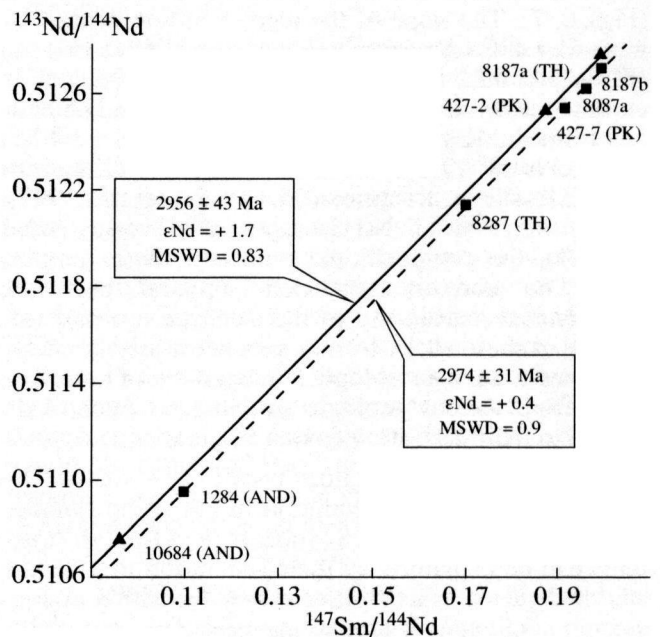
Fig. 16. Sm–Nd evolution diagram for the komatiites (PK), basalts (TH), and andesites (AND) of the Hautavaara greenstone structure.

geochemical type I (ΣHREE = 0.4–2.5 chondr., ΣFeO = 10–12 wt %, and Al_2O_3 = 2–6 wt %) with chondritic HREE distribution patterns and slight LREE depletion [$(Ce/Sm)_N$ = 1.1–0.7] (Vrevsky *et al.*, 1996). The combination of such a character of REE distribution with high positive εNd suggests that the mantle reservoir had been depleted long before komatiite generation, and, by

the moment of komatiite melt formation, this reservoir was homogeneously mixed with a less depleted lower mantle component.

Type DM_2. The most depleted εNd(T) values (from +4.7 to +3.8) above the line of Nd isotopic evolution of the DM reservoir (DePaolo and Wasserburg, 1976) were obtained for the komatiites of the Kamennoozero,
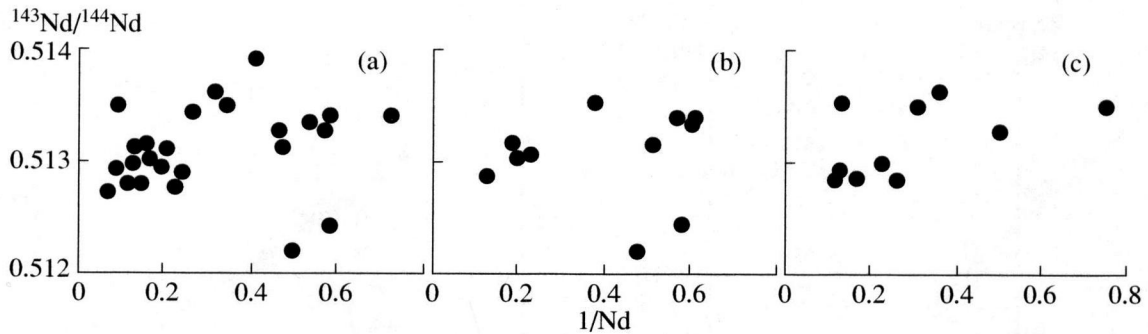
Fig. 17. Diagram ^{143}Nd/^{144}Nd versus 1/Nd for the komatiites and tholeiitic basalts of the greenstone belts of the Kola Peninsula, northern Karelia, and western Karelia. (a) Polmos-Porosozero, Ura Guba, Hizovaara, and Kostamuksha structures, 2860 ± 190 Ma. (b) Polmos-Porosozero, Ura Guba, Hizovaara, and Korva Tundra structures, 2882 ± 190 Ma. (c) Kostamuksha structure, 2889 ± 100 Ma.

Sovdozero, and Koikari greenstone structures (Table 4), which are confined to the oldest age group (3.05–2.9 Ga) of the Baltic shield belts (Fig. 2). The komatiites of the Kamennoozero greenstone structure correspond to a type II geochemical source, which is depleted in LREE and shows chondritic HREE contents (2.0–3.0 chondr.) and Ti/Zr similar to that of the DM (Figs. 6, 7). The slope of the regression line defined by these four samples corresponds to an age of 3016 ± 64 Ma (MSWD = 0.22 and εNd = +4.4) (Fig. 15), which is close to the Sm–Nd isochron age of basalts and komatiites from the Kamennoozero structure, 3034 ± 84 Ma (Puchtel *et al.*, 1999), and tholeiites from the Kenozero and Shilosskaya structures (Sochevanov *et al.*, 1991). In the diagram of Nd isotopic ratio versus 1/Nd (Fig. 17), the compositional points of these samples reveal no correlation, which supports both the geochemical plausibility of the isochron age and formation of these rocks from a geochemically homogeneous melt. Such an isotopic homogeneity of komatiite melts from various geologic structures is most likely related to their derivation from a single mantle source.

The relatively high values εNd(T) > + 4.0 that lie above the line of DM evolution in komatiite samples from the Kamennoozero, Sovdozero, and Koikari structures can be explained by their generation in a mantle source depleted as a result of earlier formation of considerable amounts of crustal material. This material is probably represented by the tonalite–trondhjemite gneisses and basic schists of the adjacent Vodlozero block, which have a U–Pb isochron zircon age of 3.14 ± 0.03 Ga and a Sm–Nd model age higher than 3.3 Ga (εNd from −2 to +1) (Lobach-Zhuchenko *et al.*, 1993). The same mechanism of the "short-term ultradepletion" of mantle composition was inferred for an age of 3.0 Ga in southern Africa and Western Australia (Krapez, 1993).

Types UM and EM. A number of komatiite samples from the Vedlozero–Segozero greenstone belt of Karelia (Koikari, Sovdozero, Hautavaara, and Palaya Lamba structures) show low εNd(T) values (from +1.8 to +0.4, Table 4). The occurrence of such values in

mantle-derived igneous complexes could be related to various reasons: (1) melt contamination by crustal material; (2) migration of Sm and Nd during metamorphism; (3) melt generation in an enriched mantle reservoir (EM); and (4) melting of previously solidified eutectoid mantle melts.

Let us consider the relevance of these alternative mechanism for the low εNd(T) values in the komatiites of the Baltic shield.

(1) A change in εNd(T = 2900) from +4.0 in one part of melt derived from the depleted mantle (L_{DM}) to the values between +1.8 and +1.4 that were observed in some komatiites from the Vedlozero–Segozero greenstone belt by the assimilation of x parts of crustal rocks is described by the following equation of two-component mixing:

$$x = C_{Nd}(L_{DM})[\varepsilon Nd(PK)$$
$$- \varepsilon Nd(DM)]/C_{Nd}(\gamma)[\varepsilon Nd(\gamma) - \varepsilon Nd(PK)],$$

where C_{Nd} is the Nd concentration in the mixing component (contamination); L_{DM} is the melt with εNd(T = 2900) = +4.0; PK is the komatiites of the Hautavaara and Palaya Lamba structures; and γ is the crustal rocks whose isotopic characteristics were accepted after Lobach-Zhuchenko *et al.* (1993).

In order to produce the desired change in εNd, the komatiite melt must assimilate 10–12% of underlying dacite with εNd = −1.3, Ti = 4200 ppm, Zr = 220 ppm, and Y = 10 ppm or 5–8% of tonalite with εNd = −0.3, Ti = 2100 ppm, Zr = 143 ppm, and Y = 9 ppm. However, under such degrees of contamination, the komatiites could not have retained their Ti/Zr and Zr/Y trends (Fig. 14), and their enrichment in LREE would have been 2–3 times higher than the observed value [(La/Sm)$_N$ = 1.2–1.3].

(2) A decrease in εNd(T) is also possible through REE migration due to superimposed processes, which was shown for the komatiites of the Tipasjarvi and Suomussalmi greenstone belts in eastern Finland (Tourpin *et al.*, 1991). Svecofennian tectonic and thermal events disturbed also the Pb–Pb isotopic system of potassium

feldspar and the Rb–Sr isotopic system of biotite in these komatiites. However, in the case under consideration, such changes in the Sm–Nd isotopic system probably did not occur, because even the much more sensitive to metamorphic processes K–Ar$_{(Amf)}$ and Pb–Pb$_{(Rock)}$ isotopic systems of the komatiite-hosting volcanic complexes of the Hautavaara and Palaya Lamba structures preserved their Archean age values (2540 ± 40 and 2940 ± 62 Ma, respectively; Ovchinnikova *et al.*, 1994).

(3) Excluding the possibility of the influence of the two former mechanisms (contamination and secondary alteration) on the εNd(T) of komatiites from the Vedlozero–Segozero greenstone belt, one has to suppose that the mantle source of komatiites from this structure corresponded in isotope geochemical characteristics to mantle reservoirs enriched to varying degrees (EM) and/or undepleted (UM). This supposition is supported by two Sm–Nd isochrons for bulk rocks (komatiites and tholeiites) with ages of 2937 ± 56 Ma (εNd(T) = +1.5 and MSWD = 0.7) and 2980 ± 99 Ma (εNd(T) = +0.3 and MSWD = 0.05) (Fig. 14), which coincide in general with the Sm–Nd isochron ages of komatiites, basalts, and andesites from the Koikari and Palaya Lamba structures (Svetov and Huhma, 1999). The isochron dependencies obtained by us for the komatiites of these structures (Fig. 15) more adequately reflect the isotopic characteristics of their mantle sources, because, first, the basalts and andesites of the Palaya Lamba structure are not comagmatic in their geochemical characteristics; and, second, the absence of a correlation between the Nd isotopic composition (^{143}Nd/^{144}Nd) and reciprocal Nd concentration (1/Nd, Fig. 17) in the komatiite samples from the Vedlozero–Segozero greenstone belt suggests their generation from two independent mantle reservoirs with εNd (T) of +1.7 and +0.4.

Thus, the established connection of the komatiites of the Vedlozero–Segozero greenstone belt to two independent mantle sources and the lack of evidence for isotopic mixing and geochemical contamination with underlying rocks and older complexes provide new insights into the geochemical kinship between the mantle reservoirs of all types of volcanics from the lower part of the section of the Hautavaara structure. In the Sm–Nd evolution diagram (Fig. 16), the points of isotopic compositions of komatiites and published data (Ovchinnikova *et al.*, 1994) for basalts, andesites, and dacites form two linear trends with slopes corresponding to ages of 2956 ± 43 Ma (εNd = +1.7 and MSWD = 0.83) and 2974 ± 31 Ma (εNd = +0.4 and MSWD = 0.9). These data allow us to state with confidence that two isotopic types of mantle reservoirs with different initial Nd isotopic signatures contributed to the generation of all varieties of volcanism of the initial stage of structure development.

Thus, the examples with low initial ^{143}Nd/^{144}Nd ratios allow us to suppose the existence of two isotopic

types of mantle reservoirs (sources) with different degrees of enrichment, εNd(T) of +1.7 and +0.4, for the parental komatiitic magmas of the greenstone belts of central Karelia. The appearance of such reservoirs could be related to homogeneous mixing in varying proportions of the components of the normal depleted mantle (DM$_1$), which served as a source for the komatiites of the Kola Peninsula and northern Karelia, or strongly depleted mantle (DM$_2$), which gave rise to some komatiites from central Karelia, with the primitive (PM) or undepleted lower mantle (UM), which supplied the komatiite melts of western and part of central Karelia. The latter separated from the lower mantle at an early stage (~3.0 Ga) of mantle plume ascent.

GEOCHEMICAL MODELING OF THE PROCESSES OF KOMATIITE PETROGENESIS

Any petrological interpretation of the geochemical types and groups of komatiites of the Baltic shield must take into account the following general tendencies in the chemical evolution of mantle sources and magma generation conditions.

(1) **LREE depletion (Ce/Sm and Ce/Yb < 1)** could be related to the following factors: (a) melting of the depleted mantle, whose composition is usually calculated by subtraction of the average continental crust composition from the 40 vol % of the primitive mantle (PM) corresponding to the average silicate Earth composition (e.g., McDonough and Sun, 1995); (b) repeated melting of the mantle source after removal of an initial liquid corresponding in composition to basalt or komatiitic basalt, which also results in an increase in the total REE content in the melt relative to the source. In principle, such a petrogenetic mechanism is geochemically equivalent to the melting of depleted mantle sources. In these two cases, the isotopic compositions of melts would be different, because the former mechanism implies a considerable time gap between the processes of mantle differentiation into the crustal matter and the depleted mantle and generation of komatiite magma.

(2) **HREE depletion [(Gd/Yb)$_N$ > 1]** could be related to (a) garnet fractionation during global mantle differentiation in the Early Archean (4.6–4.4 Ga) (Gruau *et al.*, 1990); (b) mantle melting at high pressure (P > 16 GPa) near the $Px \longrightarrow Mj$ (majorite) phase transition (10% Mj in the residue increases the Gd/Yb ratio of melt by 70%) (Ohtani, 1990); and (c) varying cotectic relationships of garnet and pyroxene in mantle material at moderate pressures ($P \cong 12$ GPa).

(3) **Different average chondrite-normalized total HREE contents (ΣHREE$_N$) at a given magnesium content of melts:** (a) variations in ΣHREE$_N$ within 2.0–3.0 can be explained by varying degrees of melting (±5%) of the DM source at constant cotectic mineral proportions in the depleted mantle (DM) and REE contents twice as high as those of chondrites; (b) changes

in $\Sigma HREE_N$ (less that 1.0 and more than 3.0) in komatiites can be due to their derivation from primitive (PM) and enriched (EM) sources, respectively.

In the case of mixing of two or several source types in the magma generation area shortly before melt zone formation, liquids can be produced with transitional (mixed) isotopic geochemical characteristics.

Such a relative diversity of possible reasons for the appearance of various geochemical and petrological types of mantle melts with application to the distinguished isotopic and geochemical groups of komatiites and their deep sources in the Baltic shield can be described only by means of petrological and geochemical computer modeling, which allows us to account for the above-described processes of deep petrogenesis and their constraints.

The modeling of trace and rare earth element behavior in the processes of equilibrium partial melting relies on modern theoretical and experimental data on the regularities of incompatible element partitioning between melt and solid phases. The evolution trends of mantle melts were calculated using equations describing REE variations during batch melting (Allegre and Minister, 1978), REE partition coefficients for cotectic mineral phases at various *P-T* parameters (Nykanen, 1994), quantitative mineral proportions in mantle reservoirs at varying depth (McKenzie and O'Nions, 1991), and chondritic initial contents of trace and rare earth elements in the mantle (McDonough and Sun, 1995).

Modeling of REE Behavior in Mantle Melting Processes

Theoretical and experimental data on the petrogenesis of komatiites and compositions of their mantle sources suggest that the following factors are most important for the interpretation of possible and observed variations in the geochemical and isotopic compositions of komatiite melt and must be accounted for in model calculations: the mineralogical composition of mantle material as a function of depth (pressure) of melting, the cotectic proportions of minerals entering the melt, and the degree of mantle source depletion.

The same data place the following constraints on the parameters of komatiite petrogenesis: liquidus temperature of komatiite melts $T = 1530–1730°C$; degree of direct equilibrium partial melting of the mantle $F = 20–50\%$; and pressure $P \leq 8.0$ GPa, because at greater depths (at $T = 1200°C$), the density of liquidus olivine (Fo_{93}) becomes equal to that of the melt of peridotitic komatiite of type B4 (Belingwe) (Agee and Walker, 1993).

The following chondrite-normalized contents and ratios of rare earth elements were accepted for various model mantle reservoirs (sources):

primitive mantle (PM), 0.5–1.0 chondr.;

undepleted (normal) mantle (UM), 2.0 chondr.;

depleted mantle (DM_1) – $(Ce/Sm)_N$ = 0.9; and

depleted mantle (DM_2) – $(Ce/Sm)_N$ = 0.8.

Four main models were calculated for the petrogenesis of komatiite melts:

(1) melting of primitive (0.5–1.0 chondr.) garnet-bearing (*Mj*) peridotite (CHUR) at $P > 14$ GPa;

(2) melting of undepleted mantle material at various depths:

—normal garnet (*Mj*) peridotite at $P = 9–14$ GPa,

—normal garnet peridotite at $P = 2.5–4.0$ GPa, and

—garnet-free peridotite at $P < 2.5$ GPa;

(3) melting of depleted (by previous 2% melt extraction) normal garnet peridotite (DM_1 type) at $P = 4–9$ GPa; and

(4) melting of depleted (by previous 5% melt extraction) normal garnet-free mantle peridotite (DM_2 type) at $P = 2.5–4.0$ GPa.

The models of melt generation with $P > 9$ GPa were explored in order to gain general insights into the possible compositions of melts within the high-temperature axial zone of an ascending adiabatic mantle plume, which could segregate from the host material when the plume reached pressure levels below 8 GPa. When such melts reach the surface, they provide the most adequate information on the composition of lower mantle plume material, because the axial part is least affected by interaction with the surrounding upper mantle.

Description of Models

Model 1. Melting of primitive (0.5–1.0 chondr.) garnet-bearing (Mj) peridotite at P > 14 GPa

This model implies melting at very large depths (>450 km) in the transitional zone between the upper and lower mantle, whose mineralogy is dominated by two phases, majoritic garnet (*Mj*) and MgSiO_3 perovskite (Mg-*Pv*). It was accepted that the minerals entered the melt in the cotectic proportion $Mj_{30\%}$ + Mg-$Pv_{70\%}$. Changes of cotectic proportions by ±25% do not affect significantly the composition of model melts and solid residues. As a model assumption, the geochemical composition of the mantle was taken as 0.5 chondr., which corresponds to the composition of undepleted primitive material of the lower mantle arriving into the melting zone during plume ascent.

The distribution of REE in the model liquids that were derived by batch partial melting at $F = 2–46\%$ is strongly fractionated up to $F = 30\%$, whereas higher degree melts are characterized by chondritic distribution of LREE and strong depletion in HREE (Fig. 18), which is related to the retention of majorite in the solid residue within the whole range of degree of mantle melting. It is characteristic that the melts generated at $F > 35\%$ show approximately chondritic $\Sigma LREE$ and $\Sigma HREE$ contents from 0.9 to 0.4 chondr. Correspondingly, the solid residues of the $Mj–(Mg-Pv)$ mantle have chondrite-normalized REE contents much lower than one within the whole range of degree of melting and enriched HREE distribution spectra.

Model 2a. Melting of undepleted normal (2 chondr.) garnet (Mj) peridotite at P = 9–14 GPa

These calculations (Fig. 18) simulate the melting of upper mantle material surrounding an ascending mantle plume at depths of 300–450 km. In this model the behavior and distribution of REE in melts and complementary residues are identical to those of model 1, because melting is controlled up to $F = 45\%$ by the presence of majorite in the solid residue even after olivine disappearance from the cotectic assemblage. The melts of komatiitic compositions ($F > 10\%$) are characterized by higher total REE contents (5–8 chondr.).

Model 2b. Melting of normal undepleted garnet peridotite at P = 2.5–4.0 GPa

This variant of model calculations (Fig. 18) simulates the passage of a plume through the shallower levels (130–300 km) of undepleted mantle ($Ol_{0.60} + Opx_{0.20} + Cpx_{0.08} + Grt_{0.12}$). Within a melting range of 1–20%, the compositions of melts and complimentary solid residues are controlled by the cotectic relationship $Ol_{0.05} + Opx_{0.05} + Cpx_{0.36} + Grt_{0.54}$. The melts show very strongly fractionated REE distribution patterns, $(Ce/Yb)_N \cong 100$, and much higher total REE contents as compared to model 2a (Fig. 18). Garnet disappears from the cotectic assemblage at $F > 20\%$ practically simultaneously with clinopyroxene. This changes abruptly REE distribution in the melt to an unfractionated "chondritic" character. The total REE content of melt changes from 70 chondr. at $F = 21\%$ to 7–8 chondr. at $F = 55\%$.

The modeling of major-element melt composition suggests that, already at small degrees of melting ($F > 5\%$), MgO content corresponds to Al-undepleted komatiites (MgO > 20 wt %). The abundance of Al_2O_3 in the melt decreases from 15 wt % at $F = 2\%$ to 9 wt % at $F = 50\%$, which is in agreement with the experimental results on the melting of Tinaquillo lherzolite, garnet lherzolite KLB-1, and spinel lherzolite HK-66.

Model 2c. Melting of normal undepleted garnet-free peridotite at P < 2.5 GPa

The compositions of model melts (Fig. 18) derived by melting of undepleted mantle peridotite ($Ol_{0.60} + Opx_{0.26} + Cpx_{0.14}$) when the plume reaches the shallowest levels (<130 km) is controlled by the cotectic proportions (a) $Ol_{0.15} + Opx_{0.35} + Cpx_{0.5}$ at $F = 1–30\%$ and (b) $Ol_{0.3} + Opx_{0.7}$ at $F > 30\%$. Melting with cotectic assemblage (a) produces liquids with a slight LREE enrichment $[(Ce/Sm)_N = 5–12]$ and an unfractionated HREE distribution. When clinopyroxene is completely consumed by the melt [cotectic (b)], the distribution of REE becomes flat, and chondrite-normalized REE contents vary from 10 to 2.5–3.0.

The major-element compositions of highly magnesian (MgO > 25 wt %) melts derived by melting ($F = 30–60\%$) with cotectic proportions (b) are characterized by relatively uniform Al_2O_3 contents (between 6.0 and 5.3 wt %) and a decrease in CaO content from 9.0 to 5.2 wt %. They correspond to the composition of Al-depleted komatiite and are consistent with the experimental results on mantle peridotite melting.

Model 3. Melting of normal depleted (by previous 2% melt extraction) garnet-bearing peridotite (type E-DM) at P = 4–9 GPa

This model (Fig. 18) describes the process of melting of depleted upper mantle peridotite at depths of 130–300 km during the further ascent of the plume. The melting of garnet-bearing mantle peridotite ($Ol_{0.63} + Opx_{0.22} + Cpx_{0.06} + Grt_{0.09}$) is controlled by the cotectic assemblage $Ol_{0.05} + Opx_{0.05} + Cpx_{0.36} + Grt_{0.54}$ at moderate degrees of batch partial melting ($F = 1–15\%$). The melts are characterized by unfractionated LREE distribution patterns and HREE depletion with total chondrite-normalized REE contents of 7–10.

At a degree of melting of $F > 15\%$, the behavior of REE in the melts is controlled by the cotectic proportion $Ol_{0.30} + Opx_{0.70}$. After disappearance of garnet and clinopyroxene from the cotectic assemblage, the REE distribution patterns show a slight depletion in LREE and unfractionated HREE. The total chondrite-normalized REE contents of the melts vary from 2 to 12.

Model 4. Melting of normal depleted (by previous 5% melt extraction) garnet-free ($Ol_{0.62} + Opx_{0.26} + Cpx_{0.12}$) peridotite (type N-DM) at P = 2.5–4.0 GPa

This model (Fig. 18) describes melting of the most depleted upper mantle at depths of 50–130 km. When the degree of melting is between 2 and 22%, the REE distribution patterns of the melts are controlled by the cotectic proportion $Ol_{0.15} + Opx_{0.35} + Cpx_{0.5}$. The REE distribution spectrum of melts remains flat (chondritic) up to $F = 10\%$ and shows a slight depletion in LREE at $F = 12–22\%$ and a total REE content of 8–12 chondr. The chondrite-normalized REE contents of the complementary solid residues vary from 1.0 to 0.5, and there is a slight depletion in LREE within the whole range of degree of melting ($F = 2–22\%$).

At higher degrees of batch partial melting ($F > 24\%$), clinopyroxene is completely consumed by the melt, and melting is controlled by the cotectic proportion $Ol_{0.30} + Opx_{0.70}$. The change of cotectic assemblage does not fundamentally affect the character of REE distribution in melt and only reduces the total chondrite-normalized REE content from 8 to 1.5. The complete dissolution of clinopyroxene in the melt results in a significant depletion of the solid residue in LREE, and the total chondrite-normalized REE content decreases from 0.1 to 0.05.

Model 5. Melting of depleted garnet-bearing peridotite contaminated by 2% of melt (F = 20%) derived from a garnet-free primitive mantle material

These calculations simulate the most hypothetical and complex mechanism including mixing in the plume head zone, when it reaches the lithospheric mantle,
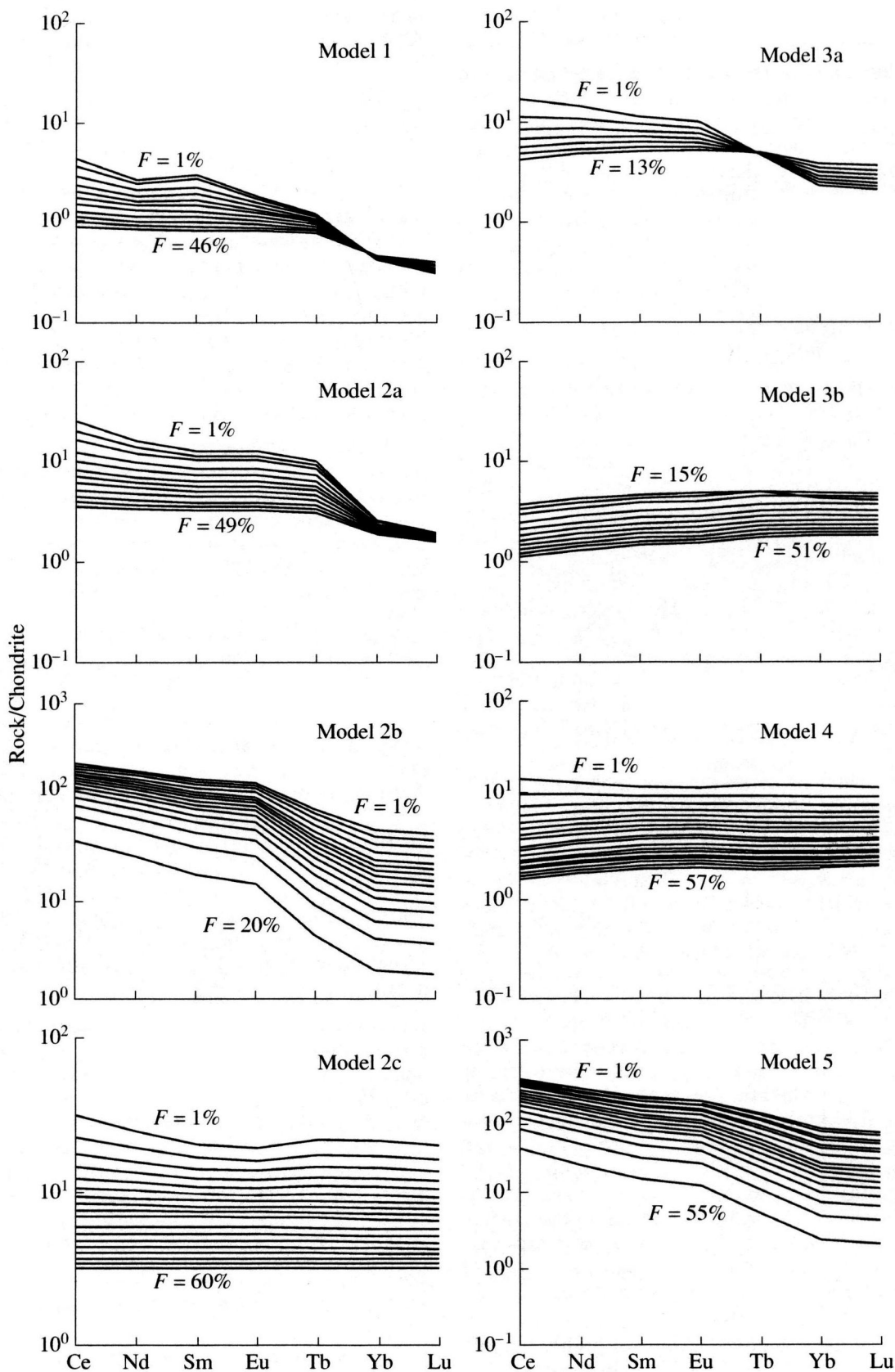
spreads, and descends into the deeper levels of the surrounding upper mantle.

The most remarkable feature of the model melts (Fig. 18) is a strongly fractionated REE distribution, $(Ce/Yb)_N > (Ce/Sm)_N$, whereas the complimentary solid residues are characterized by almost chondritic proportions of all REE. This model is distinguished from all other cases considered by the possibility of producing melts with the highest values of both $(Ce/Yb)_N$ and $(Ce/Sm)_N$.

Comparative Analysis of the Geochemical Compositions of Komatiites and the Results of Modeling of Magma Generation Processes in the Mantle

In order to facilitate the comparison of REE behavior during the derivation of basic and ultrabasic melts from the mantle with the compositions and REE distribution patterns of komatiites, three elements were selected (Ce, Sm, and Yb) as representatives of light, medium, and heavy lanthanides, respectively. Minimizing in such a way the excess geochemical information, we constructed a simple and informative diagram (Figs. 19a, 19b), which describes genetic relations between various mantle derivatives and their sources (liquid products of batch partial melting and complementary solid residues).

Melts derived from garnet-free and garnet-bearing mantle materials are efficiently discriminated in the $Ce_N–Sm_N–Yb_N$ diagrams (Figs. 19a, 19b). For instance, melts from a garnet-free material show similar $(Ce/Sm)_N$ and $(Ce/Yb)_N$ values, whereas melts derived from a garnet-bearing material (garnet is retained in the solid residue) show much higher variations in $(Ce/Yb)_N$ and less significant changes in $(Ce/Sm)_N$. It should be noted that the trends of solid residue evolution in these diagrams can be regarded as evolution trends of mantle material depleted to varying extents by previous episodes of batch partial melting, which is clearly seen when one compares the evolution paths of partial melt compositions in model 2c with the composition of initial material in model 4 (Fig. 19b).

Since the chemical evolution of melts and solid residues is illustrated in these diagrams by the relationships of light, medium, and heavy REE, they cannot reflect the distinguished mantle sources of komatiites with different HREE contents.

A comparison of the results of model calculations with the REE distribution patterns in the komatiites of the Baltic shield in this diagram (Fig. 19c) allows us to distinguish at least four types of mantle sources with different mineralogical compositions and degrees of depletion in light lanthanides.

(1) **Normal undepleted garnet-bearing mantle peridotite (model 2b).** The compositions of komatiites from the Kola Peninsula (Polmos-Porosozero, Ura Guba, and Korva Tundra structures) and some komatiites from northern Karelia (Hizovaara structure) form two fields (M-5 and M-2b, Fig. 19c), which coincide with model melt evolution trends for (a) garnet-bearing undepleted mantle peridotite at $P = 4–9$ GPa and (b) garnet-bearing material preliminary contaminated with the melt derived from garnet-free mantle peridotite, respectively.

(2) **Depleted (DM_1) by previous 2% melt extraction garnet-bearing mantle peridotite (model 3).** This trend of model melt compositions corresponds to field M-3 (Fig. 19c) formed by the compositions of komatiites from western Karelia (Kostamuksha structure) and most of the samples from eastern Finland.

(3) **Primitive garnet-free mantle peridotite ($P = 2.5–4.0$ GPa, model 2c).** This source is most appropriate for the komatiites of the Vedlozero–Segozero greenstone belt of central Karelia (Hautavaara, Palaya Lamba, and Sovdozero structures; field M-2c; Fig. 19c).

(4) **Strongly depleted (DM_2) garnet-free mantle source (model 4).** The compositions of komatiites from the Kamennoozero (eastern Karelia), Koikari, and in part Sovdozero (central Karelia) structures form field M-4, which corresponds to the evolution trend of the compositions of solid residues produced by melting of depleted (by previous 5% melt extraction) garnet-free mantle peridotite, which suggests that these komatiites were generated by melting of a mantle material previously depleted by extraction of more than 5% melt. The uncertainty area at the intersection of the compositional fields of model M-3 and M-4 melts comprises a number of komatiite compositions from the Kostamuksha structure. However, since the volcanism of western Karelia is much younger (by >100 m.y.) than that of central Karelia and the isotopic compositions of the komatiites are significantly different, their petrogenesis is considered here within model M-3.

Fig. 18. Chondrite-normalized REE distribution patterns for the model melts derived by varying degrees (F) of batch partial melting of various geochemical types of mantle materials. Model 1: $F = 1–46\%$, primitive mantle (1.0 chondr.) at $P > 14$ GPa; model 2a: $F = 1–50\%$, undepleted (2 chondr.) majorite-bearing mantle at $P = 9–14$ GPa; model 2b: $F = 1–20\%$, normal (1 chondr.) garnet-bearing mantle at $P = 2.5–4.0$ GPa; model 2c: $F = 1–60\%$, normal (2 chondr.) garnet-free ($Ol + Opx + Cpx$) mantle at $P < 2.5$ GPa; model 3a: $F = 1–50\%$, normal (2 chondr.) mantle peridotite depleted by previous 2% melt extraction ($Ol_{63} + Opx_{22} + Cpx_6 + Grt_9$, cotectic $Ol_5 + Opx_5 + Cpx_{36} + Grt_{54}$) at $P = 4–9$ GPa; model 3b: $F = 1–50\%$, normal (2 chondr.) mantle peridotite depleted by previous 2% melt extraction ($Ol_{75} + Opx_{25}$, cotectic $Ol_{30} + Opx_{70}$) at $P = 4–9$ GPa; model 4: $F = 2-51\%$, normal mantle peridotite depleted by previous 5% melt extraction (composition $Ol_{62} + Opx_{26} + Cpx_{12}$ and cotectic $Ol_{15} + Opx_{35} + Cpx_5$ at $F = 1–22\%$; composition $Ol_{77} + Opx_{23}$ and cotectic $Ol_{30} + Opx_{70}$ at $F = 25–57\%$) at $P = 2.5–4.0$ GPa; and model 5: depleted garnet-bearing mantle material preliminary contaminated with 2% melt ($F = 20\%$) derived from primitive (1 chondr.) garnet-free peridotite.
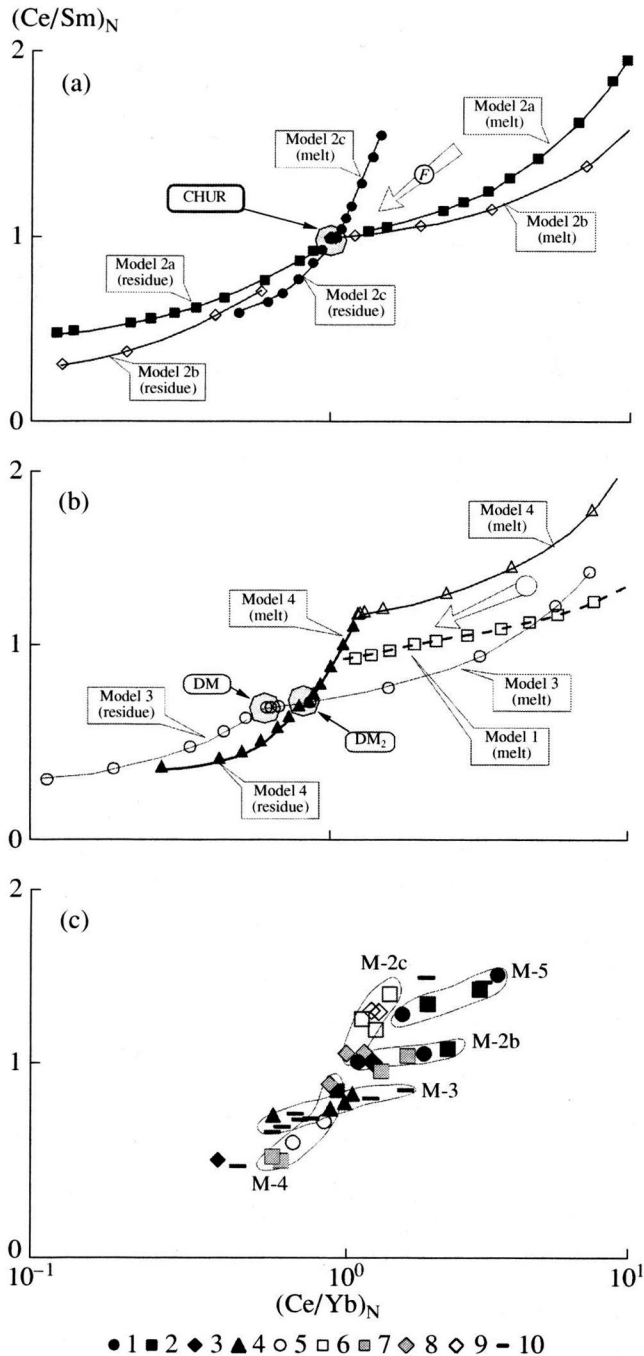
$(Ce/Sm)_N$

(a)

Model 2c (melt)

CHUR

Model 2a (melt)

Model 2a (residue)

Model 2b (melt)

Model 2c (residue)

Model 2b (residue)

F

(b)

Model 4 (melt)

Model 4 (melt)

Model 3 (residue)

DM

DM$_2$

Model 3 (melt)

Model 1 (melt)

Model 4 (residue)

(c)

M-2c

M-5

M-2b

M-3

M-4

10^{-1} 10^0 10^1

$(Ce/Yb)_N$

●1 ■2 ◆3 ▲4 ○5 □6 ▤7 ◈8 ◇9 – 10

Fig. 19. (a), (b) Modeling of the processes of batch partial melting of some geochemical types of mantle materials (CHUR, DM$_1$, and DM$_2$) and (c) position of the komatiites of the Baltic shield relative to the model melting trends. Structures: (1) Polmos-Porosozero, (2) Ura Guba, (3) Hizovaara, (4) Kostamuksha, (5) Kamennoozero, (6) Hautavaara, (7) Koikari, (8) Sovdozero, (9) Palaya Lamba, and (10) eastern Finland.

DISCUSSION AND CONCLUSIONS

The investigation of komatiites from the Baltic shield allowed us to reveal a number of specific features and regularities in the evolution of their geochemical and isotopic compositions in time, which reflect both lateral and vertical heterogeneities in the composition of their mantle sources and some genetic characteristics of the generation of parental komatiitic magmas (Figs. 20a–20c).

The variations in the geochemical characteristics of komatiites are related to the varying thermodynamic conditions of generation of their primary melts, which is demonstrated by the comparison of the regional features of komatiite compositions with the experimental results on melting of various mantle materials and the calculated values of the liquidus temperatures of komatiites.

It was found that the Kola Peninsula komatiites were derived at the highest temperatures (1620–1720°C) and depths, the Kostamuksha structure komatiites showed lower temperatures (1580–1650°C), and the lowest temperature were obtained for the komatiites of eastern and central Karelia (1570–1590°C). In general, these results suggest that the mantle source of komatiite melts was overheated by 250–350°C relative to the mantle temperature according to Richter's (1988) model.

The lateral heterogeneity of upper mantle composition beneath the Baltic shield corresponds in a number of parameters to the age zoning of volcanism in the Lopian greenstone belts:

—the oldest mantle source of komatiites from eastern and central Karelia (3050–2900 Ma) had a normal composition with a ΣHREE of 1.5–2.5 chondr.;

—the lowest ΣHREE of 0.3–1.5 chondr. is characteristic of the source of komatiites with an age of 2900–2800 Ma from the Kola Peninsula and northern Karelia; and

—the youngest (2790–2750 Ma) mantle source with the maximum ΣHREE = 4.5–6.5 chondr. was established for the komatiites of eastern Finland and western Karelia.

The Nd isotopic signatures of komatiites suggest the existence of several mantle isotopic reservoirs, sources of parental komatiite melts (Table 5), each of which was characterized by a specific degree of depletion and time of parental komatiite melt segregation.

The compositions of the oldest (3.05–2.9 Ga) komatiites from the greenstone belts of central and eastern Karelia suggest the most heterogeneous isotopic composition of their mantle sources: the most depleted ($εNd(T) ≈ +4.2 ± 0.2$) source (DM$_2$) of komatiite melts, which segregated from the mantle $3016 ± 64$ Ma ago, is typical of the komatiites of eastern Karelia and part of central Karelia (Sovdozero and Koikari structures); and the least depleted source ($εNd(T) ~ +0.3$) was deduced for the komatiites and high-magnesia basalts of the Vedlozero–Segozero greenstone belt of central Karelia, which separated from their mantle source $2980 ± 99$ Ma ago. In addition, the majority of komatiites from central Karelia with a bulk-rock Sm–Nd isochron age of $2937 ± 56$ Ma suggest a mantle source with transitional isotopic
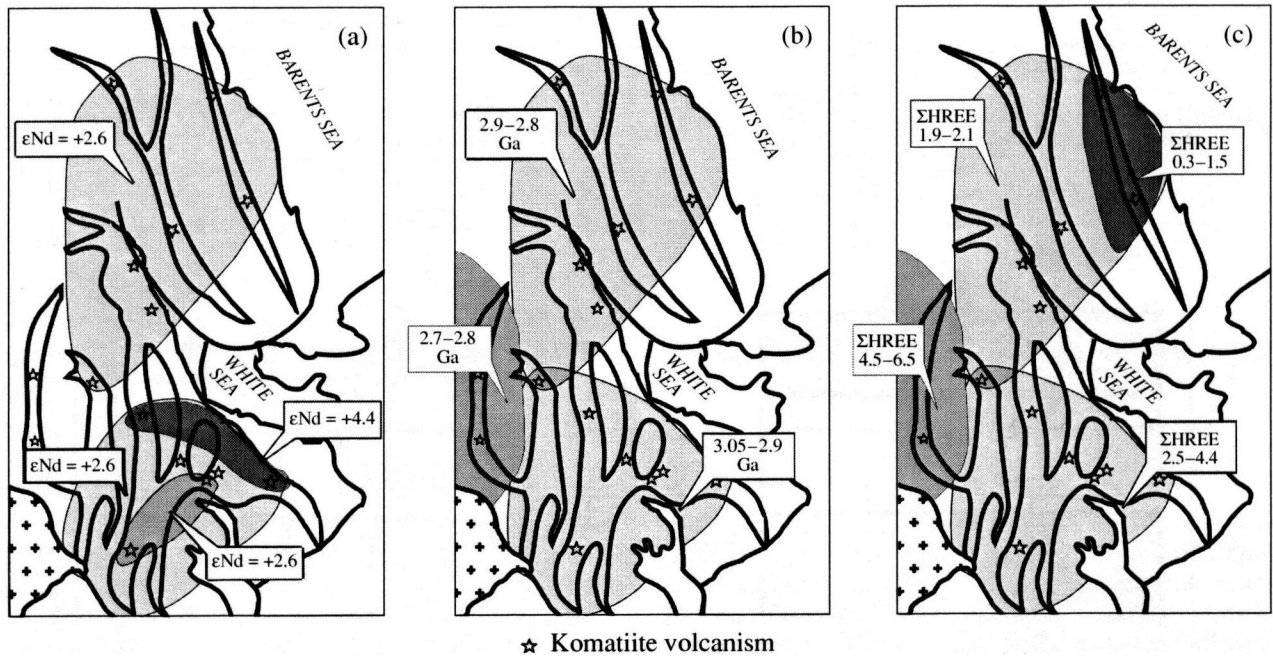
☆ Komatiite volcanism

Fig. 20. Schemes of the lateral heterogeneity of mantle volcanism occurrence in the Archean greenstone belts of the Baltic shield. (a) Nd isotopic composition (εNd) of the mantle sources of komatiites. (b) Isotopic age (Ga) of volcanism. (c) Chondrite-normalized total HREE contents in komatiites.

characteristics, $\varepsilon Nd(T) \approx +1.5 \pm 0.2$, which probably resulted from mixing of isotopic components from the depleted (DM_1) and primitive or undepleted (PM or UM) mantle reservoirs.

The source of komatiites from the Kola Peninsula, northern Karelia, and part of western Karelia (Kostamuksha structure) was represented by a mantle material of the DM_1 type ($\varepsilon Nd(T) = +2.5 \pm 0.2$). The isotopic similarity of the mantle sources of komatiites from these greenstone belts is reinforced by the fact that they form a regional isochron with an age of 2870 ± 90 Ma, which coincides within errors with internal isochrons obtained from the komatiite samples of the Kola Peninsula (Polmos-Porosozero, Ura Guba, and Korva Tundra structures) and the Kostamuksha structure separately (2882 ± 190 Ma, $\varepsilon Nd = +2.8$ and 2889 ± 100 Ma, $\varepsilon Nd = +2.3$, respectively). Thus, the komatiite melts of the greenstone belts of the Kola Peninsula, northern Karelia, and part of western Karelia separated from their mantle sources later (within errors) than those of central and eastern Karelia within the age interval of the development of greenstone belts of the second age group.

The petrological and geochemical modeling of petrogenetic processes in the mantle producing ultrabasic melts of various depths and comparison of these results with the observed compositions of Archean komatiites from the Baltic shield allowed us to distinguish at least four types of mantle sources differing in mineralogical composition and degree of depletion in light lanthanides: (1) normal undepleted garnet-bearing

mantle peridotite (UM); (2) depleted (DM_1) by previous 2% melt extraction garnet-bearing mantle peridotite; (3) primitive garnet-free mantle peridotite (PM) ($P = 2.5$–4.0 GPa); and (4) strongly depleted (DM_2) by previous 5% melt extraction garnet-free mantle material.

There are several lines of evidence suggesting that the interpretation of the established characteristics of komatiites must be based on the plume-tectonic paradigm of lithosphere development in the granite–greenstone terranes of the Baltic shield in the Late Archean (3.1–2.6 Ga) (Vrevsky *et al.*, 1996). The most important among them is the occurrence in a single greenstone structure of komatiites bearing isotopic geochemical signatures of different mantle sources [$[Ce/Yb]_N$ from 0.8 to 1.2 and $\varepsilon Nd(T)$ from $+0.3$ to $+4.4$], their polychronous character (from 3.05 to 2.75 Ga), varying depths of generation, and overheating (1530–$1730°C$) (Table 6).

Table 5. Isotopic types of mantle sources for primary komatiite melts and time of their separation

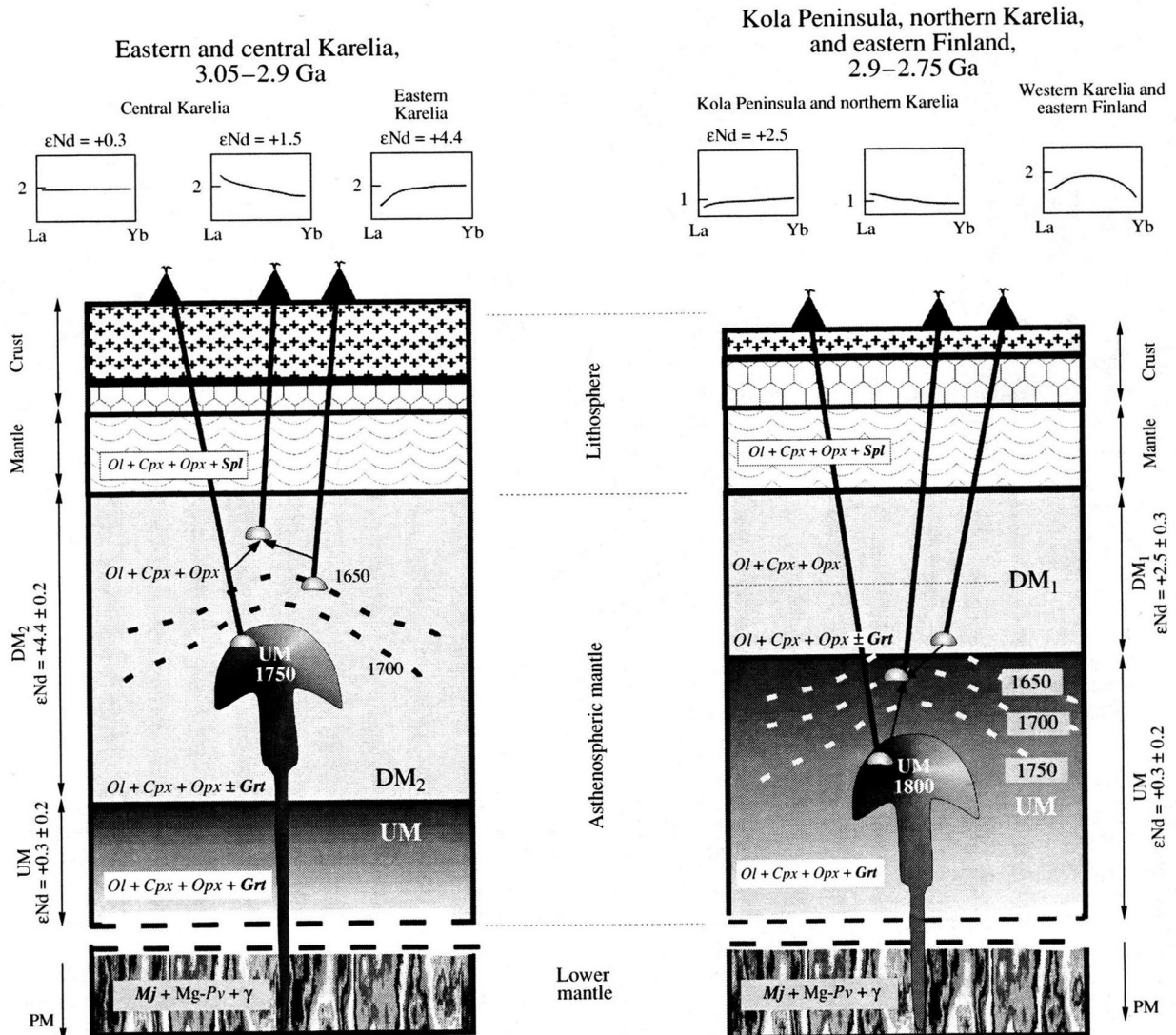| Source type	$\varepsilon Nd(T)$	Region	Age, Ma
DM_2	+4.4	Eastern and part of central Karelia	3016 ± 64
UM or EM	+0.3 +1.5	Central Karelia	2980 ± 99 2937 ± 56
DM_1	+2.5	Kola Peninsula, northern Karelia, and western Karelia	2870 ± 90

Fig. 21. Schematic petrological and isotopic geochemical model for the structure of the Archean lithosphere and asthenosphere beneath the Baltic shield in the zone of komatiite melt generation.

The data obtained were generalized in a schematic model of the evolution of two mantle plumes of different ages (I and II). This model explains most adequately the established regularities in the evolution of mantle sources of komatiites (Fig. 21). Proceeding from the concept of McCullach and Bennett (1994) and McCullach (1996) on the possible simultaneous and interrelated existence of different crustal volumes and upper mantle reservoirs depleted to varying degrees, we accepted in our model the isotope geochemical heterogeneity (layering) of the Archean upper mantle beneath the Baltic shield in the zone of komatiite melt generation.

The incipient magmatism of greenstone belts related to plume evolution was controlled by the depth of adiabatic plume melting, heterogeneous composition of the surrounding lower mantle, and the temperature gradient in the overheated plume material. The mantle plume material was probably represented by undepleted peridotite (UM, $\varepsilon Nd(T) = +0.3 \pm 0.2$) ascending from the zone of anomalous thermodynamic processes at the boundary between the lower and upper mantle (~670 km).

The earliest stage (3.1–1.0 Ga) of plume I development is reflected in the heterogeneity of the sources of komatiites from eastern and central Karelia. One of such sources was strongly depleted garnet-free ($Ol + Cpx + Opx$) mantle peridotite (DM$_2$, $\varepsilon Nd(T) = +4.4 \pm 0.2$), which was a residue from a previous partial melting event ($F = 10–5\%$) of the undepleted garnet peridotite of the upper mantle. These processes of early differentiation and melting of the asthenospheric mantle with the formation of considerable volumes of

Table 6. Characteristics of model mantle plumes

Characteristics	Mantle plume I			Mantle plume II		
	Central and eastern Karelia			Kola Peninsula, northern Karelia, and western Karelia		
Age, Ga	3.05–2.9			2.9–2.75		
Liquidus temperature of komatiites (T, °C)	1570–1590			1620–1720 (1580–1650)		
Depth level of komatiite melt generation (GPa)	2.5–4.0			4.0–9.0		
Mantle source	DM_2	UM	$(DM_2 + UM)$	DM_1	UM	$(DM_1 + DM_2)$
$\varepsilon Nd(T)$	+4.4	+0.3	+1.5	+2.5	+0.3	
Cotectic proportion in the melting zone	$Ol_{60} + Opx_{26} + Cpx_{14}$; $Ol_{62} + Opx_{26} + Cpx_{12}$			$Ol_{60} + Opx_{20} + Cpx_8 + Grt_{12}$; $Ol_5 + Opx_5 + Cpx_{36} + Grt_{54}$		

crustal material and complementary depleted mantle were responsible for its garnet-free mineralogy and strongly depleted isotopic signature. The second type of komatiite source was represented by undepleted plume material ($\varepsilon Nd(T)$ = +0.3 ± 0.2), and the corresponding primary melts were not in equilibrium with pyropic garnet. This circumstance can be interpreted as an indicator of a shallow level of mantle plume ascent (P < 2.5 GPa). The most ambiguous in a petrological context is one of the mantle source of komatiites from central Karelia with OIB-type isotopic characteristics ($\varepsilon Nd(T)$ = +1.7 ± 0.2), because the related komatiitic melts show no clear geochemical individuality. The explanation of this phenomenon must be looked for therefore in the isotopic geochemistry of mantle reservoirs. As was shown above, the absence of evidence for crustal contamination permits two alternative mechanisms: (1) homogeneous mixing in varying proportions of undepleted (UM, $\varepsilon Nd(T)$ = +0.3 ± 0.2) material from the axial part of the plume head with the enclosing depleted mantle (DM_2, $\varepsilon Nd(T)$ = +4.4 ± 0.2), which usually occurs in the zone around the frontal spherical part of the ascending plume; and (2) melting of zones, areas, or lenses of mantle peridotites that experienced previous partial melting to a smaller degree than the major volume of the enclosing strongly depleted mantle (DM_2). The solid residue of such melting events may show primary $^{143}Nd/^{144}Nd$ values transitional between those of the PM and DM_2 types of mantle reservoirs.

A distinctive feature of the petrogenesis of primary komatiite melts of the younger (2.9–2.8 Ga) greenstone belts of the Kola Peninsula and northern Karelia is their equilibrium with pyropic garnet in the zone of magma formation and a normal depleted mantle source (DM_1, $\varepsilon Nd(T)$ = +2.5 ± 0.3). In addition, the geochemical parameters of these komatiite melts suggest that part of them was obviously derived from undepleted garnet-bearing mantle peridotite in the highest temperature axial part of plume II.

The komatiites of geochemical group Ia from the Kola Peninsula with unique geochemical characteristics

[$\Sigma HREE$ ~1.5–0.3, $(Gd/Yb)_N$ ~ 1.0, and $(Ce/Sm)_N$ = 0.2–1.2) play a key role in our petrogenetic scheme. The petrological and geochemical modeling of melting of the mantle with chondritic initial geochemical characteristics did not produce melts with such low contents of heavy lanthanides. Probably, the reason for the appearance of such melts must be looked for in some specific composition of the lower mantle material that makes up the axial part of the plume.

Finally, it is necessary to point out that our petrological and geochemical models for the generation of mantle melts are schematic to a certain extent, because they are based on the limited experimental data on mantle peridotite melting at high temperatures and pressures and the limited database on the natural and experimental partition coefficients of trace and rare earth elements between melt and high-pressure cotectic mineral phases of the mantle. Nonetheless, the authors believe that the combined utilization of quantitative petrological and isotopic methods is a necessary prerequisite for obtaining a system of constraints of direct, often actualistic, correlations of the geochemical and isotopic characteristics of Early Precambrian complexes with their geodynamic nature.

ACKNOWLEDGMENTS

REFERENCES

Agee, C.B. and Walker, D., Olivine Flotation in Mantle Melt, *Earth Planet. Sci. Lett.*, 1993, vol. 114, pp. 315–324.

Allegre, C.J. and Minster, J.F., Quantitative Models of Trace Elements Behavior in Magmatic Processes, *Earth Planet. Sci. Lett.*, 1978, vol. 38, pp. 1–25.

Arndt, N.T., Archean Komatiites, in *Archean Crust Evolution,* Condie, K.C., Ed., Amsterdam: Elsevier, 1994, part 1, pp. 11–44.

DePaolo, D.J. and Wasserburg, G.J., Nd Isotopic Variations and Petrogenetic Models, *Geophys. Res. Lett.*, 1976, vol. 3, pp. 249–252.

Dobretsov, N.L., Kirdyashkin, A.G., and Kirdyashkin, A.A., *Glubinnaya geodinamika* (Deep-Seated Geodynamics), Novosibirsk: Sib. Otd. Ross. Akad. Nauk, 2001.

Ganguli, D., Crystal Chemical Aspects of Olivine Structures, *N. Jb. Mineral. Abh.*, 1977, vol. 130, pp. 303–318.

Girnis, A.V., Ryabchikov, I.D., and Bogatikov, O.A., *Genezis komatiitov i komatiitovykh bazal'tov* (The Genesis of Komatiites and Komatiitic Basalts), Moscow: Nauka, 1987.

Green, D.H., Petrogenesis of Archean Peridotitic Magmas in Implications for Archean Geothermal Gradients and Tectonics, *Precambrian Plate Tectonics*, 1981, part 19, pp. 469–489.

Gruau, G., Chauve, C., Arndt, N.T., and Cornichet, J., Aluminum Depletion in Komatiites and Garnet Fractionation in the Early Archean Mantle: Hafnium Isotopic Constraints, *Geochim. Cosmochim. Acta*, 1990, vol. 54, pp. 3095–3101.

Hart, J.T., The Structural Morphology of Olivine, *Can. Mineral.*, 1978, vol. 16, pp. 175–186.

Hatton, C.J., The Effect of Pressure, Temperature, and Composition of Fe and Mg between Olivine, Orthopyroxene, and Liquid: An Appraisal of the Reversal in the Normal Fractionation Trend in the Bushveld Complex, *Contrib. Mineral. Petrol.*, 1984, vol. 86, pp. 45–53.

Hirose, K. and Kushiro, I., Partial Melting of Dry Peridotites at High Pressures. Determination of Compositions of Melts Segregated from Peridotite Using Aggregates of Diamond, *Earth Planet. Sci. Lett.*, 1993, vol. 114, no. 4, pp. 477–490.

Jahn, B.-M., Bernard-Griffiths, J., Charlit, R., *et al.*, Nd and Sr Isotopic Composition and REE Abundances of Cretaceous MORB (Holes 417D and 418A, Legs 51, 52, and 53), *Earth Planet. Sci. Lett.*, 1980, vol. 48, pp. 171–184.

Klassifikatsiya magmaticheskikh (izverzhennykh) porod i slovar' terminov (Classification of Magmatic (Igneous) Rocks and a Glossary), Moscow: Nedra, 1997.

Komatiites, Arndt, N.T. and Nesbet, E.G., Eds., London: Allen and Unwin, 1982.

Komatiity i vysokomagnezial'nye vulkanity rannego dokembriya Baltiiskogo shchita (Early Precambrian Komatiites and Highly Magnesian Volcanics in the Baltic Shield), Leningrad: Nauka, 1988.

Krapez, B., Sequence Stratigraphy of the Archean Supracrustal Belts of the Pilbara Block, Western Australia, *Precambrian Res.*, 1993, vol. 60, pp. 1–45.

Lobach-Zhuchenko, S.B., Chekulayev, V.P., Sergeev, S.A., *et al.*, Archean Rocks from Southeastern Karelia (Karelian Granite Greenstone Terrane), *Precambrian Res.*, 1993, vol. 62, pp. 375–397.

McCullach, M.T. and Bennett, V.E., Progressive Growth of the Earth's Continental Crust and Depleted Mantle, *Geochim. Cosmochim. Acta*, 1994, vol. 58, pp. 4717–4738.

McCullach, M.T., Isotopic Constraints on the Age and Early Differentiation of the Earth, *J. Royal Soc. W. Australia*, 1996, vol. 79, pp. 131–139.

McDonough, W.F. and Sun, S.-S., The Composition of the Earth, *Chem. Geol.*, 1995, vol. 120, pp. 223–253.

McKenzie, D. and O'Nions, R.K., Partial Melt Distributions from Inversion of Rare Earth Element Concentrations, *J. Petrol.*, 1991, vol. 32, pp. 1021–1091.

Nesbet, E.G., Bickle, M.J., and Martin, A., The Mafic and Ultramafic Lavas of the Belingwe Greenstone Belt, Rhodesia, *J. Petrol.*, 1977, vol. 18, pp. 521–566.

Nesbet, E.G., Cheadle, M.J., Arndt, H.T., and Bickle, M.J., Constraining Potential Temperature of Archean Mantle: A Review of the Evidence from Komatiites, *Lithos*, 1993, vol. 34, pp. 291–307.

Nykanen, V.M., Vuollo, J.I., Liipo, J.O., and Piirainen, T.A., Transitional (2.1 Ga) Fe-Tholeiitic–Tholeiitic Magmatism in the Fennoscandian Shield Signifying Lithospheric Thinning during Paleoproterozoic Extensional Tectonics, *Precambrian Res.*, 1994, vol. 70, pp. 45–65.

Ohtani, E., Majorite Fractionation and Genesis of Komatiites in the Deep Mantle, *Precambrian Res.*, 1990, vol. 48, pp. 195–202.

Ovchinnikova, G.V., Matrenichev, V.A., Levchenkov, O.A., *et al.*, U–Pb and Pb–Pb Isotope Studies of Acid Volcanics from the Hatavaara Greenstone Structure, Central Karelia, *Petrologiya*, 1994, vol. 2, no. 3, pp. 266–281.

Puchtel, I.S., Hofmann, A.W., Amelin, Yu.V., *et al.*, Combined Mantle Plume-Island Arc Model for the Formation of the 2.9 Ga Sumozero–Kenozero Greenstone Belt, SE Baltic Shield: Isotope and Trace Element Constraints, *Geochim. Cosmochim. Acta*, 1999, vol. 63, pp. 3579–3595.

Puchtel, I.S., Hofmann, A.W., Mezger, A.W., *et al.*, Oceanic Plateau Model for Continental Crustal Growth in the Archean: A Case Study from the Kostomuksha Greenstone Belt, NW Baltic Shield, *Earth Planet. Sci. Lett.*, 1998, vol. 155, pp. 57–74.

Richter, F.M., A Major Change in the Thermal State of Earth at the Archean–Proterozoic Boundary: Consequences for the Nature and Preservation of Continental Lithosphere, *J. Petrol. Spec. Lithosphere Issue*, 1988, pp. 39–52.

Ryabov, V.V., Olivines from Siberian Traps as Indicators of Petrogenesis and Ore Mineralization, *Tr. Inst. Geol. Geokhim. Sib. Otd. Ross. Akad. Nauk*, no. 795, Novosibirsk: Nauka, 1992.

Scarrow, J.H. and Cox, K.G., Basalts Generated by Decompressive Adiabatic Melting of a Mantle Plume: A Case Study from the Isle of Skye, NW Scotland, *J. Petrol.*, 1995, vol. 36, pp. 3–22.

Smol'kin, V.F., *Komatiitovyi i pikritovyi magmatizm rannego dokembriya Baltiiskogo shchita* (Early Precambrian Komatiitic and Picritic Magmatism of the Baltic Shield), St. Petersburg: Nauka, 1992.

Sochevanov, N.N., Arestova, N.A., Matrenichev, V.A., *et al.*, First Data on the Sm–Nd Age of Archean Basalts from the Karelian Granite–Greenstone Area, *Dokl. Akad. Nauk SSSR*, 1991, vol. 318, no. 1, pp. 175–180.

Svetov, S.A. and Khukhma, Kh., Geochemistry and Sm–Nd Isotopic Study of Archean Komatiite–Tholeiite Assemblages from the Vedlozero–Segozero Greenstone Belt, Central Karelia, *Dokl. Ross. Akad. Nauk*, 1999, vol. 369, pp. 261–263.

Tourpin, S., Gruau, G., Blais, S., *et al.*, Resetting of REE, and Nd and Sr Isotopes during Carbonatization of Komatiite Flow from Finland, *Chem. Geol.*, 1991, vol. 90, pp. 15–29.

Tronnes, R.G., Canil, D., and Wei, K., Element Partitioning between Silicate and Coexisting Melts at Pressures of 1–27 GPa and Implications for Mantle Evolution, *Earth Planet. Sci. Lett.*, 1992, vol. 111, pp. 241–255.

Vaganov, V.I. and Sokolov, S.V., *Termobarogeokhimiya ul'traosnovnykh paragenezisov* (Studying Inclusions in Ultramafic Mineral Assemblages), Moscow: Nedra, 1988.

Velinskii, V.V. and Bannikov, O.L., *Oliviny al'pinotipnykh giperbazitov* (Olivine from Alpine-Type Ultrabasic Rocks), Novosibirsk: Nauka, 1986.

Vrevskii, A.B. and Krymskii, R.Sh., Sm–Nd Systematics and Geochemistry of Archean Peridotite Komatiites from the Baltic Shield, *Dokl. Ross. Akad. Nauk*, 1997, vol. 352, no. 1, pp. 80–82.

Vrevskii, A.B., Rybakov, S.I., Efimov, M.M., *et al.*, A Comparative Analysis of Geological Structure and the Development of Greenstone Belts in the Baltic and Southern Indian Shields, *Geotektonika*, 1996, no. 5, pp. 43–54.

Vrevsky, A., Krimsky, R., and Svetov, S., Isotopic (Nd, O) and Geochemical (REE) Heterogeneity of the Archean Mantle, Baltic Shield, in *Precambrian Crustal Evolution in the North Atlantic Regions*, Brewer, T.S., Ed., *Geol. Soc. Spec. Publ.*, 1996, no. 112, pp. 43–53.

Wei, K., Tronnes, R.G., and Scarfe, C.M., Phase Relations of Aluminium-Undepleted and Aluminium-Depleted Komatiites of Pressures 4–12 GPa, *J. Geophys. Res.*, 1990, vol. 95, pp. 15817–15828.

Zelenokamennye poyasa fundamenta Vostochno-Evropeiskoi platformy (Geologiya i petrologiya vulkanitov) (Greenstone Belts in the Basement of the East European Platform: Geology and Petrology of the Volcanic Rocks), Leningrad: Nauka, 1988.